We deeply thank the two anonymous referees for the valuable comments and suggestions, which help us largely improve the quality of the manuscript. All of the referee's concerns have been addressed, and the detailed responses to each comment are shown as following.

Response to referee #1

General points:

Comment #1: Several sections in the paper are too long and descriptive. Condensing these areas would improve the paper.

There are several statements within the text that require references for validation and the authors should pay attention to this.

Response: Please see the responses to the specific points #1 and #7.

Comment #2: Whilst the model has been validated against observational climate data and radiation data, the results would benefit from comparison to any cloud microphysical data that is available from satellite or observational studies that could provide some context and comparison for the changes in cloud ice and cloud liquid that occur when the semi-direct and indirect effects are included in the model.

Response: In the first part of this paper (also in discussion, available at https://www.atmos-chem-phys-discuss.net/acp-2017-754/), a new treatment for online calculating the ice nucleation process involving dust particles has been implemented in to WRF-Chem. The validation for the simulated ice water content has been described in that manuscript by applying satellite observations (CALIPSO and MODIS), so it is not included in this manuscript. It turned out that the inclusion of the ice nucleation process involving dust particles improved the simulation of the atmospheric ice water content.

Comment #3: Following on from the above point, please could you address the following point: How sure can you be that using a different microphysics scheme would give you the same results given the uncertainty in mixed phase cloud microphysics.

Response: Currently, there is no other microphysics scheme in WRF-Chem that contains an ice nucleation process involving dust particle, so we cannot say that the same results can be produced by using other microphysics schemes, especially during dust events.

However, introducing a treatment for calculating ice nucleation process involving dust, which is what we have done in the first part of this paper, is essential to accurately evaluating the effects of dust particles, and the comparison with the observations has demonstrated that the simulation of the atmospheric ice water content is improved by taking this process into account.

Specific points:

Comment #1: L42 - 43 – 'Dust particles are recognized as effective ice nuclei…': please add some relevant references here.

Response: The references have been added.

Comment #2: L47 – assessing its replace with assessing the

Response: Revised.

Comment #3: L48 – 'Many observational and modeling studies… ': Without any specific references this sentence (and others like it) are not necessary and just detract from the point of the section.

Response: The sentence has been deleted.

Comment #4: L47 – L62 – The writing and flow of this section could be improved.

Response: The section has been rewritten.

Comment #5: L53 – 'Recently:…': This word is superfluous, start the sentence with Several studies…

Response: Revised.

Comment #6: Table 1 – Any variable component that is the same in all 4 four experiments does not need to be included in the table, the lines from Soil dataset to Chemistry mechanism could all be removed from the table and this information given in the caption of the table, or a footnote or in the main text. The table is excessively long with this information and would be more informative with just the relevant information.
Response: The redundant content in Table 1 has been deleted.

Comment #7: L94 - L95 '… the Shao's dust emission scheme...': This should read 'Shao'. Also please provide a reference for reproduction of the dust emissions over East Asia.
Response: Revised, and the citation has been added.

Comment #8: L104 – 'The configurations…were mostly the same as ...': Not appropriate language. Perhaps abbreviate to: Because no dust is simulated in NO-AER/NO-CLOUD and NO-AER/CLOUD these simulations do not include a dust emission scheme, etc
Response: Revised.

Comment #9: Section 3 – Model Validation. This section was overly descriptive and felt repetitive towards the end. Please consider rewriting this.
Response: The section has been rewritten to remove redundant content.

Comment #10: Figures 1- 4 (but specifically Figures 1 & 2): It is hard to visually compare the simulation output with the observational data because the observational data does not include ocean data but the simulations do. Outlining the region where observational data is available on the simulation output would make this clearer.
Response: We have replotted these figures to make it clearer for reading.

Comment #11: In all figures the individual color scales could be replaced by 1 large vertical scale bar for more clarity.
Response: We have replaced the small legends with general larger ones in Fig. 1–6, and Fig. 12. But as the plots in other figures (Fig. 7-8, Fig. 13) do not share the same color legend, we cannot apply a general color scale for these figures, so we keep the original legends for these figures in the revised manuscript.

Comment #12: L150, L167 and other places: 'a significant improvement' 'not so significant'. Throughout the text phrases like this are misnomers, you have not included any evidence of significance testing and so these statements are not appropriate as the comparisons are subjective. Either consider calculating significance, include what significance testing was carried out or change the language.
Response: We have modified the statement to exclude the description of significance.

Comment #13: L197 – Figure 6 is mentioned before Figure 5, this is confusing, reorder the figures.
Response: It was a mistake to mention Figure 6 before Figure 5 at the start of section 4 ("…within the atmosphere over East Asia during the simulation period are shown in Figures 6 and 7…", it should be "…Figure 5 and 6"), we have revised it in the updated manuscript.

Comment #14: Section 4 – Please start this section with a sentence similar to used for the caption in Table 2.
Response: Revised.

Comment #15: L235 – L236 – Could the size fraction of dust play a role here? With coarse dust near the source responsible for more LW absorption?
Response: Yes, we have revised the sentence to be "…due to the absorption of LW radiation by the thick dust layer with large fraction of coarse particles in the atmosphere."

Comment #16:L290 – typo in downwelling all-sky

Response: Revised.

Comment #17: L291 – L292 – within the atmosphere (remove in).
Response: Revised.

Comment #18: L337 – Are there any observational records that could be compared against the cloud liquid water and cloud ice water path values in the models?
Response: Yes. The comparison has been done in the first part of this paper for validating the performance of the model in simulating the atmospheric ice water content.

Comment #19: L350 – Similarly here is there any observational data for cloud droplet number?
Response: We cannot find any kind of observational data for cloud droplet number.

Comment #20: L360 - The peak at 6 km doesn't look like a peak. It's an increase that is sustained for several km.
Response: Revised.

Comment #21: Figure 13 – Consider showing the precipitation anomalies as a percentage change in precipitation to better convey the data.
Response: It can be done but the figures will be messy. As there are many areas where there is no precipitation in the CTRL run, the percentage cannot be calculated for these areas. Therefore, we keep the original figures in the updated manuscript.

Response to referee #2

General comments:

Comment#1: My main question is regarding the setup of the sensitivity tests. My understanding is that in addition to dust as aerosols, there are also other aerosols included (coming from C1 ACPD Interactive comment Printer-friendly version Discussion paper the GOCART scheme, with should include as far as I know, sulfates, sea-salts, elemental and organic carbon). When describing the NO-AER and AER runs, the authors state that NO-AER are conducted without dust, and with aerosol radiative feedback turned off. The way I read this is that radiative feedbacks for all aerosols (sulfates, carbon, seasalt and dust) are turned off. In the same manner, when aerosol radiative feedbacks are turned on (AER runs), I read this as aerosol feedbacks for all aerosols (not only dust) is turned on. If this is true, I think there is a problem with the sensitivity tests, as evaluating the differences between NO-AER and AER actually includes impacts from all aerosols, and not only dust. In this case, more sensitivity tests are needed, where only the radiative effect of dust is turned on or off, and not all aerosols. If I am misunderstanding, and the radiative effects of the remaining aerosols (sulfates, sea-salt and carbon) are always on, then this needs to be explained in the paper. For example, instead of calling the different runs for NO-AER and AER, call them NO-DUST and DUST instead.

Response: No other emissions were included in this study except for dust, that is to say, the GOCART aerosol model produced only dust emission for further calculation, so only the effects of dust on the weather system were considered.

We have replaced “NO-AER” and “AER” with “NO-DUST” and “DUST” in the revised manuscript to avoid confusion.

Comment #2: Nothing is said about homogeneous freezing in this paper. Is homogeneous freezing of deliquesced aerosols included, which is an important part for cirrus production? Or are the NO-AER runs with a constant 1 per Liter as IN the only way to produce ice in the scheme? If homogeneous freezing is not included, I believe these runs highly overestimate the effect of dust, as increased dust concentration in cirrus regions can actually cause decreases in ice crystal concentration through the competition between homogeneous and heterogeneous freezing process. If homogeneous freezing of deliquesced aerosols are included, then please state that in the paper for clarification.

Response: Apart from heterogeneous freezing, Homogeneous freezing of deliquesced aerosols is considered and determined following the Koop’s parameterization (with the background aerosol concentration set to 1/L). We did mention it in the first part of the paper, but omitted it in this manuscript. We have clarified the parameterization schemes used for ice nucleation process in section 2 of the revised manuscript.

Comment #3: There are several citations missing in this paper. Make sure all work that is referred to are cited.

Response: Please see the responses to the specific minor comments #3, #4, #5, #6.

Comment #4: In general, I suggest using IN (or INP) as an acronym for ice nuclei, since this is commonly used in the ice (or INP) community.

Response: Revised.

Minor comments:

Comment #1: Page 3, line 45: Precipitation should be singular and not precipitations.

Response: Revised.

Comment #2: Page 4, line 60: Rephrase “very rare work”

Response: “very rare work” has been replaced by “only limited work”, with citations added.

Comment #3: Page 4, line 66: The correct name for the Thompson aerosol aware scheme is the Thompson-Eidhammer aerosol aware scheme. Further, a citation to their 2014 paper is needed here.

Response: Another referee, Dr. Gregory Thompson, also mentioned this problem. We have replaced “aerosol-aware Thompson scheme” into “Thompson-Eidhammer scheme” in both manuscripts. Also the citation has been added.

Comment #4: Page 4, Line 67: A citation is needed for the first Part of the series. After searching and finding this paper I am surprised that the authors did not cite it, as they are the authors of the first part of the series as well.

Response: Thanks for reminding. The citation has been added (see the response to the next comment).

Comment #5: A short description of the calibration factor cf should be included here. Also a short description of the effect of setting RH to 100 % in relation to the ice nucleation parameterization should be explained in this paper. And which ice nucleation scheme is used? Actually, I believe the authors could include a section, summarize briefly part I of the series where they include a short description of the GOCARTThompson implementation and their findings.

Response: We have included a short description of the calibration factor and the effect of lowering RH to 100% in section 2 of the revised manuscript. And we have also included a section about the parameterization schemes used for the ice nucleation process, as well as the work done in the done in part I in section 1 of the updated manuscript. The citation to the first part of the series has been added at these two places.

Comment #6: Page 5, line 94: A citation for Shao's dust emission scheme is needed.

Response: The citation has been added.

Comment #7: Page 8, line 171: Replace "observed" with "observations"

Response: Revised.

Comment #8: Page 8, line 190: Replace "reproducing" with "reproduced"

Response: Revised.

Investigating the role of dust in ice nucleation within clouds and further effects on the regional weather system over East Asia

Part II: modification of the weather system

Lin Su[1], and Jimmy C.H. Fung[2, 3]

[1] School of Science, Hong Kong University of Science and Technology, Hong Kong, China

[2] Division of Environment, Hong Kong University of Science and Technology, Hong Kong, China

[3] Department of Mathematics, Hong Kong University of Science and Technology, Hong Kong, China

Correspondence to: Lin Su (lsu@connect.ust.hk)

Keywords: East Asian dust; radiative forcing; clouds; precipitation; regional modeling

Highlights:

The semi-direct and indirect effects of dust are more pronounced than the direct effect on the regional weather system.

The semi-direct and indirect effects of dust result in an increase in mid- to high clouds, and a reduction in low clouds.

The total precipitation is reduced over most of China, but increased over South China by up to 20% or more.

Abstract. An updated version of the Weather Research and Forecast model coupled with Chemistry (WRF-Chem) was applied to quantify and discuss the full effects of dust on the meteorological field over East Asia during March and April 2012. The performances of the model in simulating the short-wave and long-wave radiation, surface temperature, and precipitation over East Asia are improved by incorporating the effects of dust in the simulations. The radiative forcing induced by the dust-enhanced cloud radiative effect is over one order of magnitude larger than that induced by the direct effect of dust. The semi-direct and indirect effects of dust result in a substantial increase in mid- to high clouds, and a significant reduction in low clouds, leading to a decrease of near-surface temperature and an increase of temperature at the mid- to upper troposphere over East Asia. The spatial redistribution of atmospheric water vapor and modification of the vertical temperature profile over East Asia lead to an inhibition of atmospheric instability over most land areas, but an enhancement of atmospheric instability over South China and the ocean, resulting in a significant inhibition of convective precipitation in areas from central to East China, and a substantial enhancement of convective precipitation over South China. Meanwhile, non-convective precipitation is also reduced significantly over East Asia, as cloud droplets are hindered from growing large enough to form rain droplets, due to the semi-direct and indirect effects of dust. The total precipitation can be reduced or increased by up to 20% or more.

1 Introduction

Dust is recognized as an "essential climate variable" because it is a major component of atmospheric aerosols and has significant impacts on the weather and climate system (Solomon, 2007). East Asian dust is an important contributor to global dust emissions (Ginoux et al., 2001), and thus play a significant role in affecting the regional weather system through direct effect, semi-direct and indirect effects.

Dust particles affect the radiation budget directly by absorbing, reflecting and scattering short-wave and long-wave radiation (Satheesh et al., 2006;Seinfeld et al., 2004;Lacis, 1995). The cloud radiative effect induced by dust is referred to as the semi-direct effect of dust. Dust particles within clouds can absorb radiation and heat up the surrounding environment, leading to faster evaporation rate of cloud droplets and thus a reduction of cloud cover. The indirect effects of dust are related to dust–cloud–interaction. (Hansen et al., 1997;Perlwitz and Miller, 2010). Dust particles are recognized as effective ice nuclei (IN) and considered to play an important role in cold cloud processes (Broadley et al., 2012;Connolly et al., 2009;Sassen, 2002), leading to the variation of the ice water content in mixed-phase and ice clouds, which further affects the formation and development of clouds, as well as precipitations (Sassen et al., 2003;Targino et al., 2006;Teller and Levin, 2006;Lohmann and Feichter, 2005).

In light of the significance of dust for the weather and climate system, assessing the~~its~~ effects of dust has become increasingly important. ~~Many observational and modeling studies have aimed to quantify the various effects of dust. Due to the limited spatial and temporal availability of observational data, numerical modeling has proven an effective way to assess the effects of dust on the weather and climate system.~~On one hand, t~~T~~he direct (Mallet et al., 2009;Nabat et al., 2015a;Ge et al., 2010;Hartmann et al., 2013;Huang et al., 2009;Bi et al., 2013;Liu et al., 2011a;Liu et al., 2011b;Palacios et al., 2015;Huang, 2017) and semi-direct (Tesfaye et al., 2015;Nabat et al., 2015b;Seigel et al., 2013)~~radiative~~ effects of dust ~~worldwide~~ has being extensively studied worldwide by applying numerical methods~~using numerical methods (Mallet et al., 2009;Nabat et al., 2015a;Ge et al., 2010;Hartmann et al., 2013;Huang et al., 2009;Bi et al., 2013;Liu et al., 2011a;Liu et al., 2011b;Palacios et al., 2015;Huang, 2017)~~. ~~Recently, several studies have investigated the semi-direct effect of dust over different regions using various global and regional models (Tesfaye et al., 2015;Nabat et al., 2015b;Seigel et al., 2013).~~ ~~Unfortunately, due to the poor understanding of the dust–cloud–interaction in microphysical processes, quantifying the microphysical effect of dust remains as a difficult problem.~~ On the other hand, v~~V~~arious ice nucleation parameterizations have been implemented into global models to

Field Code Changed

Field Code Changed

estimate the importance of dust in atmospheric ice nucleation (Lohmann and Diehl, 2006;Karydis et al., 2011;Hoose et al., 2008;Zhang et al., 2014), revealing that the effect of dust as ~~ice nuclei~~IN should not be neglected in numerical models, especially in the simulations over arid regions during strong wind events (DeMott et al., 2003;Koehler et al., 2010;DeMott et al., 2015;Lohmann and Diehl, 2006;Atkinson et al., 2013). Unfortunately, ~~However, very rare~~, only limited work has been ~~done~~ carried out to investigate the indirect effects of dust on the regional weather system, ~~especially~~ especially over East Asia, which is one of the major contributors to the global dust emission in the world (Ginoux et al., 2001).

This series of study aimed to investigate the role of East Asian dust in affecting the regional weather system. In the first part of the study, The Goddard Chemistry Aerosol Radiation and Transport (GOCART) model has been coupled with the aerosol-aware Thompson-Eidhammer microphysics scheme (Thompson and Eidhammer, 2014), enabling the model to estimate the indirect effect of dust along with the direct and semi-direct effects, which improved the simulation of the ice nucleation process involving dust particles (Su and Fung, 2017). In this work, by applying an updated version of WRF-Chem, we aim to investigate the full effects of dust, including ~~the~~ direct, ~~the~~ semi-direct, and ~~the~~ indirect effects, on the regional weather system over East Asia during a dust-intensive period. ~~In the updated WRF-Chem, The Goddard Chemistry Aerosol Radiation and Transport (GOCART) model has been coupled with the aerosol-aware Thompson microphysics scheme(Thompson and Eidhammer, 2014), enabling the model to estimate the indirect effect of dust along with the direct and semi-direct effects. This is the second part of a series of studies on the role of East Asian dust in affecting the regional weather system, and also~~This is the first study to document the full effects of dust during a typical dust-intensive period over East Asia by applying an online-coupled regional numerical model.

The remainder of the manuscript is organized as follows. The model configurations is described in Section 2, followed by the model validation in Section 3. The results along with the discussion will be presented in section 4, followed by the concluding remarks in Section 5.

2 Model configurations

The simulations were performed using an updated version of WRF-Chem based on version 3.8.1 (Grell et al., 2016). The GOCART-Thompson, which is the coupling of the GOCART aerosol model and the aerosol-aware Thompson-

Eidhammer microphysics scheme, has been implemented in the updated WRF-Chem, to evaluate the indirect effect of dust on the atmospheric ice nucleation process by serving as ~~ice nuclei~~IN. In the GOCART-Thompson microphysics scheme, ~~The implementation of GOCART-Thompson microphysics scheme was described in detail(Bigg, 1953)~~ the deposition nucleation is determined by the parameterization of Phillips et al. (Phillips et al., 2008), and the freezing of deliquesced aerosols using the hygroscopic aerosol concentration is parameterized following Koop et al. (Koop et al., 2000), with the background aerosol concentration set to be 1/L. In addition, the condensation and immersion freezing is parameterized by the DeMott2015 ice nucleation scheme, and two factors of the DeMott2015 scheme were tuned through sensitivity experiments in the first part of this study.~~,~~ c_f is a calibration factor in the DeMott2015 ice nucleation parameterization scheme, which was used for the nucleation of the heterogeneous nucleation of ice crystals by dust particles in the GOCART-Thompson scheme, and it ranges from 1 to 6. According to the results of the sensitivity experiments in Part I, the calibration factor c_f was~~is~~ set to be 4 for the simulations in this study.~~, and~~ Furthermore, it was also demonstrated that the ice water content was still underestimated by using the GOCART-Thompson scheme. To improve the simulation of the ice nucleation by dust particles, the threshold relative humidity with respect to ice (RH_i) was~~is set to be~~ lowered from 105% to 100% in the ice nucleation parameterization, to allow the heterogeneous nucleation of ice crystals by dust particles to occur at a lower RH_i (Su and Fung, 2017). Therefore, a threshold RH_i of 100% was for the simulations run with dust emissions in this study.

Formatted: Subscript

Formatted: Subscript

Formatted: Subscript

Formatted: Subscript

Four numerical simulations were carried out to evaluate the separate effects of dust over East Asia. The configurations for the four simulations are summarized in Table 1. The first simulation was termed ~~NO-AER~~NO-DUST/NO-CLOUD, and was conducted without dust, with both the aerosol radiative feedback and cloud radiative feedback turned off. The second simulation, ~~NO-AER~~NO-DUST/CLOUD, was also conducted without dust, with the aerosol radiative feedback turned off, but the cloud radiative feedback turned on to estimate the intrinsic radiative effect of cloud. The third simulation, ~~AER/~~DUST/NO-CLOUD, was conducted with the presence of dust, with the aerosol radiative feedback turned on, while the cloud radiative feedback still turned off. The difference between ~~NO-AER~~NO-DUST/NO-CLOUD and ~~AER/~~DUST/NO-CLOUD therefore represented the direct effect of dust on the radiation budget and other meteorological parameters. The last simulation, ~~AER/~~DUST/CLOUD, was conducted with the presence of dust, and with both aerosol radiative feedback and cloud radiative feedback turned on, to estimate the full effect of dust on the meteorological field over East Asia.

The important physical and chemical parameterization schemes applied for the four simulations are ~~summarized and~~

~~shown in Table 1~~as follows. The GOCART aerosol model was applied to simulate the aerosol processes (Ginoux et al., 2001;Ginoux et al., 2004). For the dust emission simulation in ~~AER/~~DUST/NO-CLOUD and ~~AER/~~DUST/CLOUD, the Shao~~'s~~ dust emission scheme (Shao, 2004;Shao et al., 2011) was applied, which had been demonstrated to closely reproduced the dust emissions over East Asia (Su and Fung, 2015). Note that no aerosol emissions were considered in the simulations other than dust. The Mellor–Yamada–Janjic (MYJ) turbulent kinetic energy scheme was used for the planetary boundary layer parameterization (Janjić, 2002, 1994); the moisture convective processes were parameterized by the Grell–Freitas scheme (Grell and Freitas, 2014); the short-wave (SW) and long-wave (LW) radiation budgets were calculated by the Rapid Radiative Transfer Model for General Circulation (RRTMG) SW and LW radiation schemes (Mlawer et al., 1997;Iacono et al., 2008); gravitational settling and surface deposition were combined for aerosol dry deposition (Wesely, 1989); a simple washout method was used for the below-cloud wet deposition of aerosols; and the aerosol optical properties were calculated based on the volume-averaging method. The newly-implemented wet scavenging scheme described in Part I of this study was used for the in-cloud wet scavenging of dust particles caused by the microphysical processes. ~~The configurations for~~As no dust was simulated in ~~NO-AER~~NO-DUST/NO-CLOUD and ~~NO-AER~~NO-DUST/CLOUD, ~~were mostly the same as for the other two simulations, but without~~these two simulations did not included a dust emission scheme, aerosol dry and wet deposition schemes, and aerosol optical schemes~~, as no dust is produced in these two simulations~~. Note that in the two NO-CLOUD simulations, a default ~~ice nuclei~~IN concentration of 1 per Liter is used for the heterogeneous ice nucleation process.

As described in the first part of this manuscript, two nested domains were used for all four simulations, the outer domain had a horizontal resolution of 27 km, covering the entire East Asia region, and the inner domain had a horizontal resolution of 9 km, covering the entire central to East China. Both domains have 40 layers, with the top layer at 50 hPa. The simulation period was March 9 to April 30, 2012, with the first eight days as "spin-up" time. Only the results from March 17 to April 30, 2012 were used for further analysis. Final reanalysis data provided by the United States National Centre~~er~~ of Environmental Prediction, with a horizontal resolution of 1°, were used for generating the initial and boundary conditions for the meteorological field. The simulations were re-initialized every 4 days, with the aerosol field being recycled, i.e., the output of the aerosol field from the previous 4-day run was used as the initial aerosol state for the next 4-day run.

3 Model validation

The simulation for dust emission was validated in Part I of this study, and the model was demonstrated to closely reproduce dust emissions over East Asia during the investigated period by comparison with comprehensive observational data. As this study focused on the modification of the meteorological field by the effects of dust over East Asia, the capability of the model in simulating the meteorological field itself over this region requires further validation.

The China meteorological forcing dataset (Yang et al., 2010;Chen et al., 2011) was used to assess the performance of the model in reproducing the spatial distribution of the meteorological field over China. The dataset was developed by the hydrometeorological research group at the Institute of Tibetan Plateau Research, Chinese Academy of Science, by merging the Princeton meteorological forcing data (Sheffield et al., 2006), the Global Energy and Water Cycle Experiment–Surface Radiation Budget (GEWEX-SRB) forcing data (Pinker and Laszlo, 1992), and the Global Land Data Assimilation System forcing dataset (Rodell et al., 2004). The dataset contains gridded observations of the near-surface temperature, precipitation rate, surface downward SW and LW radiation across China, with a spatial resolution of 0.25°, dating from 1996.

~~As this study aimed to evaluate the radiative forcing induced by dust, it was necessary to verify the performance of the model in reproducing the radiative budget. The spatial distributions for the monthly average observational SW and LW radiation from the China meteorological forcing dataset, and the simulated SW and LW radiation over East Asia from NO-AER/CLOUD and AER/CLOUD, are shown in Figures 1 and 2.~~ Note that only simulation results from ~~NO-AER~~NO-DUST/CLOUD and ~~AER/~~DUST/CLOUD are shown, as they represent the intrinsic meteorological field and the meteorological field modified by the effects of dust, respectively. For March, the comparison is restricted to the observational data from March 17 to March 31, 2012, to ensure temporal overlay with the corresponding simulation period. No observational data over the ocean were available, so the simulated results over the ocean are also omitted to simplify the comparison.

The spatial distributions for the monthly average observational downward surface SW radiation for March and April 2012 are shown in Figure 1a and b. Overall, the SW radiation was stronger in April than in March. The SW radiation was significantly higher over the West and Northwest China, due to the higher elevation of terrain over these regions, and lower over East and South China, due to the lower elevation and greater cloud coverage over those regions. The model closely reproduced the spatial distributions of the SW radiation in both months and accurately captured the trend from March to April in the simulation results from both ~~NO-AER~~NO-DUST/CLOUD and ~~AER/~~DUST/CLOUD, despite a certain overestimation, especially over coastal areas of East and South China. This overestimation was likely due to the underestimation of clouds by the model over these areas. Compared with inland areas, cloud coverage is always greater over the coastal areas of East and South China due to the abundant water vapor. Therefore, the SW radiation budget over coastal areas was more sensitive to the underestimation of clouds by the model. Nevertheless, ~~a significant~~an improvement in the simulation of the SW radiation budget over East Asia can be seen in the results from ~~AER/~~DUST/CLOUD compared with those from ~~NO-AER~~NO-DUST/CLOUD. Specifically, the SW radiation produced in ~~AER/~~DUST/CLOUD (Figure 1e and f) was substantially ~~significantly~~ lower than that produced in ~~NO-AER~~NO-DUST/CLOUD (Figure 1c and d) over China~~ as a whole~~, especially at the dust sources and surrounding areas over the north and northwest of the country, which is clearly more consistent with the observations.

~~The spatial distributions for the monthly average observational downward surface LW radiation over China for March and April 2012 are shown in Figure 2a and b.~~For downward surface LW radiation, two~~Two~~ high-value areas can be observed (Figure 2a and b). One is over Northwest China, where the Taklimakan Desert is located. The strong downward LW radiation over this region was likely due to the abundance of dust particles in the local atmosphere. ~~Dust particles suspended in the atmosphere during dust events can absorb SW radiation and heat the surrounding atmospheric layer, causing more LW radiation to be emitted downward (and upward) by this layer.~~ The other area of strong LW radiation was located over South China, which is warmer and contains more atmospheric water vapor. Water vapor is a potent greenhouse gas, which efficiently absorbs LW radiation emitted by the Earth and ~~to~~ heat the surrounding area, and thus increases the emission of LW radiation downward (and upward) by the heated atmosphere. The model accurately simulated the spatial distributions of the LW radiation over this region for both March and April in both ~~NO-AER~~NO-DUST/CLOUD (Figure 2c and d) and ~~AER/~~DUST/CLOUD (Figure 2e and f), and indeed closely captured the spatial pattern of the LW radiation over China~~ as a whole~~. ~~The difference between the results of NO-AER/CLOUD and AER/~~DUST/~~CLOUD in terms of LW radiation was not so significant as that for SW radiation. However, the slightly higher~~The LW radiation over the Gobi Desert produced by ~~AER/~~DUST/CLOUD (Figure 2e and f) is slightly higher than that produced by NO-DUST/CLOUD, ~~was more consistent with the observations,~~ indicating that the model reproduced the LW radiation budget more accurately upon taking the effects of dust into account.

~~The spatial distributions for the monthly average near-surface temperature over China from observed for March and April 2012 are shown in Figure 3a and b.~~ Similarly to the spatial distributions for the LW radiation, higher near-surface temperatures were observed over Northwest China, which is a dry, arid area, and South China, which is closer to the equator (Figure 3a and b). The spatial distributions of the near-surface temperature over this region were well reproduced by the model for both March and April in both ~~NO-AER~~NO-DUST/CLOUD (Figure 3c and d) and ~~AER/~~DUST/CLOUD (Figure 3e and f). The model accurately captured the spatial pattern of the surface temperature, and the two simulations did not ~~differ significantly~~show remarkable difference in their results.

~~The spatial distributions for the monthly average observational precipitation over China for March and April in 2012 are shown in Figure 4a and b.~~During the simulation period, t~~T~~he precipitation increased from North to South China in both months, and increased from March to April over the entire region (Figure 4a and b). The spatial patterns of precipitation in March and April were mostly reproduced by the model in both ~~NO-AER~~NO-DUST/CLOUD (Figure 4c and d) and ~~AER/~~DUST/CLOUD (Figure 4e and f), but the model underestimated the precipitation in March in both simulations, especially over central and North China. In April, the observed precipitation center was located over South China. Apart from underestimating the precipitation over Central and North China, the ~~NO-AER~~NO-DUST/CLOUD simulation predicted the precipitation center to be located in an area ~~spanning Hunan and Jiangxi (Figure 4d), which was~~ to the north of the observed center (Figure 4d), and it also ~~significantly~~ underestimated the precipitation over South China ~~compared with the observed values~~. In contrast, in the results of ~~AER/~~DUST/CLOUD (Figure 4f), the precipitation band from Hunan to the north of south China~~Jiangxi~~ was markedly weaker, while the precipitation over South China was enhanced, which was clearly much more consistent with the observations.

The foregoing comparison of the simulation results with the observational data demonstrated that the model reasonably reproduced~~ing~~ the meteorological field over East Asia. Moreover, the meteorological field was produced more accurately when the effects of dust were considered in the simulations, which consequently allows the dust-induced modification of the meteorological field to be investigated.

4 Results and discussion

4.1 Radiative effect

The radiative effect of dust particles is demonstrated by dust-induced SW, LW, and net radiative forcing at the top of the atmosphere (TOA), at the bottom of the atmosphere (BOT), and within the atmosphere (ATM) in this study.

The spatial distributions for the mean radiative forcing induced by dust at the top of the atmosphere, at the bottom of the atmosphere, and within the atmosphere over East Asia during the simulation period are shown in Figures 5~~6~~ and

6~~7~~. Note that all of the spatial distributions for radiative forcing shown in the two figures are the temporal mean over the entire simulation period. The SW radiative forcing was calculated as follows.

$$SW_{TOA} = SWDOWN_{TOA} - SWUP_{TOA} \tag{1}$$

$$SW_{BOT} = SWDOWN_{BOT} - SWUP_{BOT} \tag{2}$$

$$SW_{ATM} = SW_{TOA} + SW_{BOT} \tag{3}$$

where SW_{TOA} is the SW radiative forcing at the top of the atmosphere, and SW_{BOT} is the SW radiative forcing at the bottom of the atmosphere, both with positive values representing downwelling radiation; SW_{ATM} is the radiative forcing within the atmosphere, which is the sum of SW_{TOA} and SW_{BOT}, with positive values representing a net warming effect within the atmosphere; $SWDOWN_{TOA}$ and $SWUP_{TOA}$ are the downwelling and upwelling SW radiation at the top of the atmosphere, respectively; $SWUP_{BOT}$ and $SWDOWN_{BOT}$ are the upwelling and downwelling SW radiation at the bottom of the atmosphere, respectively.

The LW radiative forcing was calculated as follows.

$$LW_{TOA} = -LWUP_{TOA} \tag{4}$$

$$LW_{BOT} = LWDOWN_{BOT} - LWUP_{BOT} \tag{5}$$

$$LW_{ATM} = LW_{TOA} + LW_{BOT} \tag{6}$$

Where LW_{TOA} is the LW radiative forcing at the top of the atmosphere, and LW_{BOT} is the LW radiative forcing at the bottom of the atmosphere, both with positive values representing downwelling radiation; LW_{ATM} is the radiative forcing within the atmosphere, which is the sum of LW_{TOA} and LW_{BOT}, with positive values representing warming effect within the atmosphere; $LWUP_{TOA}$ is the upwelling LW radiation at the top of the atmosphere; $LWUP_{BOT}$ and $LWDOWN_{BOT}$ are the upwelling and downwelling LW radiation at the bottom of the atmosphere.

The net radiative forcing is the sum of SW and LW radiative forcing.

$$Ra_{TOA} = SW_{TOA} + LW_{TOA} \tag{7}$$

$$Ra_{BOT} = SW_{BOT} + LW_{BOT} \tag{8}$$

$$Ra_{ATM} = SW_{ATM} + LW_{ATM} \tag{9}$$

4.1.1 Clear-sky radiative forcing

The direct radiative forcing induced by dust shown in Figure 5 is also referred to as clear-sky radiative forcing, and is due to the reflection, absorption and emission of radiation by dust particles suspended in the atmosphere.

The clear-sky downwelling SW radiative forcing at the top of the atmosphere is slightly negative over most of East Asia (Figure 5a), indicating that the upwelling SW radiation at the top of the atmosphere increases due to the reflection and scattering of SW radiation by dust particles. The clear-sky SW radiative forcing at the bottom of the atmosphere is negative over most of East Asia (Figure 5g), especially over dust source regions, which suggests that the downwelling SW radiation is significantly reduced through the absorption by dust particles suspended in the atmosphere, leading to a significant net warming effect within the atmosphere (Figure 5d). Averaged over the entire simulation domain, the SW radiative forcing over East Asia is -1.22 W/m^2 at the top of the atmosphere, -2.44 W/m^2 at the bottom of the atmosphere, and 1.23 W/m^2 within the atmosphere, accounting for 0.37%, 0.97%, and 1.58% of the total clear-sky radiation budget in these three zones, respectively, as shown in Table 2.

In Figure 5b, the clear-sky downwelling LW radiation at the top of the atmosphere is slightly increased over dust source regions and downwind areas, due to the absorption of LW radiation by the thick dust layer with large fraction of coarse particles in the atmosphere. In comparison, it is slightly reduced over other areas of East Asia, indicating an increase of the upwelling LW radiation, which might be attributable to the greater emission of LW radiation by the dust layer, which in turn is due to the heating of the atmosphere caused by the absorption of SW radiation by dust particles (Figure 5d). The clear-sky downwelling LW radiation forcing is reduced at the bottom of the atmosphere (Figure 5h), which is attributed to the Earth's surface being cooler as it receives less solar radiation (Figure 5g). Combining the LW radiative forcing at the top of the atmosphere and at the bottom of the atmosphere, there is a net negative LW radiative forcing within the atmosphere (Figure 5e). Overall, the mean LW radiative forcing averaged over the entire East Asia is relatively slight, being -0.02 W/m^2 at the top of the atmosphere, 1.09 W/m^2 at the bottom of the atmosphere, and -1.07 W/m^2 within the atmosphere, accounting for 0.01%, 1.18%, and 0.63% of the total clear-sky radiation budget in those three zones, respectively.

Combining the SW and LW radiative forcing, the net downwelling clear-sky radiation at the top of the atmosphere is reduced over most of East Asia (Figure 5c). The downwelling clear-sky net radiation at the bottom of the atmosphere is reduced over most part of East Asia, especially over dust source regions and downstream areas (Figure 5i), leading to a net warming effect within the atmosphere (Figure 5f), which is slightly smaller than the warming caused by SW radiative forcing (Figure 5d). The net radiative forcing is -1.20 W/m^2 at the top of the atmosphere, -1.36 W/m^2 at the bottom of the atmosphere, and 0.15 W/m^2 within the atmosphere, accounting for 1.78%, 0.85%, and 0.16% of the total clear-sky radiation budget in those three zones.

4.1.2 All-sky radiative forcing

The all-sky radiative forcing induced by dust shown in Figure 6 is the total radiative forcing, including the radiative forcing directly induced by dust displayed in Figure 5, and that induced by the cloud radiative effect enhanced by dust. In Figure 6a, the all-sky downwelling SW radiation at the top of the atmosphere is markedly reduced over most of China compared with the clear-sky case, due to greater reflection from dust and enhanced cloud cover induced by dust over the continent. However, it is increased over the southern part of northwest Pacific, indicating less SW radiation is reflected back into space due to the cloud radiative effect, which implies less cloud cover induced by dust over this area. Compared with the clear-sky case, the all-sky upwelling SW radiation at the bottom of the atmosphere in Figure 6g is increased significantly over the continent, as more solar radiation is blocked due to the enhanced cloud cover induced by dust; however, the downwelling all-sky SW radiation at the bottom of the atmosphere is reduced over most of the West Pacific, indicating that more solar radiation that reaches the Earth's surface due to the cloud radiative effect, which also implies less cloud cover over this area. The cloud radiative effect strengthens the warming within the atmosphere over land in the all-sky case compared with the clear-sky case, while there is a slight cooling over the ocean in the all-sky case, as shown in Figure 6d, in contrast to the slight warming in the clear-sky case. Averaged over the entire simulation domain, the mean SW radiative forcing is -7.81 W/m^2 at the top of the atmosphere, and -7.87 W/m^2 at the bottom of the atmosphere (Table 2), accounting for 2.62% and 3.60% of the total all-sky radiation budget in those two zones, respectively. Within the atmosphere, the positive SW radiative forcing over land and negative SW radiative forcing over the ocean balance each other out.

Compared with the clear-sky case, the all-sky downwelling LW radiation at the top of the atmosphere is significantly increased over almost the whole of East Asia (Figure 6b), indicating much less upwelling LW radiation at the top of the atmosphere. The increase of downwelling all-sky LW radiation at the bottom of the atmosphere over land in Figure 6h is due to the greater emission of LW radiation by the warmer atmosphere, and the larger radiative forcing than that in the clear-sky case implies that the cloud cover is significantly increased over land due to dust. Conversely, there is no warming effect at the surface of the ocean, and the reduction in downwelling LW radiation over the ocean implies less cloud cover over the ocean. The combination of the direct radiative effect of dust and the cloud radiative effect enhanced by dust causes an overall increase of LW radiation within the atmosphere, leading to a warming effect, which is more pronounced over the ocean, as shown in Figure 6e. The mean all-sky LW radiative forcing over the entire simulation domain is 9.52 W/m^2 at the top of the atmosphere, accounting for 3.79% of the total all-sky LW radiation budget in that zone. The increase of the all-sky LW radiation at the bottom of the at atmosphere over land and its reduction over the ocean almost cancel each other out, leaving a mean all-sky LW radiation over the entire simulation domain of 0.25W/m^2, accounting for 0.34% of the total LW radiation budget at the bottom of the atmosphere. The mean all-sky LW radiative forcing within the atmosphere over the simulation domain is 9.26 W/m^2, accounting for 5.25% of the total all-sky LW radiation budget within the atmosphere.

Summing the SW and LW radiative forcing, the net downwelling all-sky radiation at the top of the atmosphere is reduced to the north of Central China, Korea, and Japan, and increased significantly over most of the ocean (Figure 6c). By contrast, the net dowenwelling all-sky net radiation at the bottom of the atmosphere is reduced significantly over the same land areas, and increased over most of the ocean (Figure 6i). Radiative forcing results in pronounced warming within ~~in~~ the atmosphere over East Asia as a whole (Figure 6f). Averaged over the simulation domain, the net all-sky radiative forcing is 1.70 W/m^2, -7.62 W/m^2, and 9.33 W/m^2 at the top of the atmosphere, at the bottom of the atmosphere, and within the atmosphere, accounting for 3.61%, 5.28%, and 9.61% of the total net radiation budget in those three zones, respectively.

In summary, the direct radiative effect of dust combined with the cloud radiative effect enhanced by dust causes a net loss of radiation at the Earth's surface, but a net gain of radiation within the atmosphere, leading to a cooling at the surface and lower troposphere, and a warming in mid- to upper troposphere. The radiative forcing caused by the dust-enhanced cloud radiative effect is much greater than that caused by the direct radiative effect of dust, especially for LW radiative forcing, which is highly affected by cloud cover. The LW radiative forcing caused by the dust-enhanced cloud radiative effect is one order stronger than that cased by the direct radiative effect of dust at the top of the atmosphere and within the atmosphere. The spatial distribution of radiative forcing further implies a shift of the spatial distribution of cloud cover, such that the cloud cover is likely increased over land, but reduced over the ocean due to the presence of dust, indicating a re-distribution of atmospheric water vapor over East Asia. The shift of the vertical distribution of the radiation budget, the re-distribution of atmospheric water vapor, and the modification of atmospheric stability resulting from those two processes will be discussed in more detail in later sections.

4.2 Atmospheric water vapor

4.2.1 Spatial distribution

The Semi-direct and indirect effects of dust particles lead to a modification of cloud format and cloud lifetime, and a re-distribution of atmospheric water vapor. The spatial distributions of the simulated atmospheric water vapor path, ice water path, and cloud water path from ~~NO-AER~~NO-DUST/CLOUD and ~~AER/~~DUST/CLOUD, as well as the difference (~~AER/~~DUST/CLOUD − ~~NO-AER~~NO-DUST/CLOUD) between the two simulations, are presented in Figure 7. The atmospheric water vapor path, ice water path, and cloud water path are the column sums of water vapor, ice water vapor, and cloud water vapor in the atmosphere per unit area. Note that the difference between ~~NO-AER~~NO-DUST/CLOUD and ~~AER/~~DUST/CLOUD is entirely due to the combined effects of dust, i.e., the direct effect of dust, the cloud radiative effect enhanced by dust, and the microphysical effect of dust serving as ~~ice nuclei~~IN in the atmosphere. The spatial distributions shown in Figure 7 are the mean atmospheric water vapor path, ice water path, and cloud water path averaged over the whole simulation period.

Figure 7a and b show the spatial distributions of precipitable water vapor in the atmosphere, which is equal to the total volume of the atmospheric water path in the atmospheric column, over East Asia produced from ~~NO-AER~~NO-DUST/CLOUD and ~~AER/~~DUST/CLOUD. The results from the two simulations are similar, with the same spatial pattern. The differences between the two are shown in Figure 7c, in which the precipitable water vapor is slightly reduced by less than 1 mm over most of East Asia, except for the dust source regions, over where the precipitable water vapor in the atmosphere is slightly increased. However, the increase or reduction of precipitable water vapor induced by dust, which accounts for less than 1% of the total amount of the precipitable water vapor in the atmosphere, is negligible.

The situation is different for the atmospheric ice water path. The atmospheric ice water path is lower than 1 g/m^2 over most of East Asia in the results of ~~NO-AER~~NO-DUST/CLOUD (Figure 7d), indicating that the production of ice crystals, or ice clouds, in the atmosphere is rare in the simulation without dust. By contrast, the atmospheric ice water path produced by ~~AER/~~DUST/CLOUD is substantially higher than that produced by ~~NO-AER~~NO-DUST/CLOUD over the entire simulation domain, with values higher than 20 g/m^2 over much of East Asia (Figure 7e). This corresponding to an increase of one order over vast areas, from dust source regions to the Northwest Pacific (Figure 7f), due to the dust particles serving as ~~ice nuclei~~IN in the atmosphere. Dust nuclei in the atmosphere enable the super-cooled water droplets to freeze into ice crystals at a much higher temperature and lower relative humidity.

The spatial distribution for the mean atmospheric cloud water path over the entire simulation period from ~~NO-AER~~NO-DUST/CLOUD is shown in Figure 7g, in which the cloud water path is concentrated over South China and the West Pacific, with values as high as 100 g/m^2. The spatial pattern of the atmospheric cloud water path from ~~AER/~~DUST/CLOUD in Figure 7h is qualitatively similar to that from ~~NO-AER~~NO-DUST/CLOUD, but with much lower values. The comparison of atmospheric cloud water paths between ~~AER/~~DUST/CLOUD and ~~NO-AER~~NO-DUST/CLOUD in Figure 7i shows that the atmospheric cloud water path is reduced by more than 30 g/m^2 over south China, which accounts for one third of the total atmospheric cloud water vapor over this region in the results of ~~NO-AER~~NO-DUST/CLOUD.

Figure 8 shows the spatial distributions for the mean simulated ice crystal number density and cloud droplet number density produced by ~~NO-AER~~NO-DUST/CLOUD and ~~AER/~~DUST/CLOUD over East Asia during the entire simulation period, as well as the difference between the results from the two simulations (~~AER/~~DUST/CLOUD – ~~NO-AER~~NO-DUST/CLOUD). Similar to the case in Figure 8, the simulated ice crystal number density increases substantially when the ice nucleation process is enhanced by dust particles serving as ~~ice nuclei~~IN. Compared with that produced by ~~NO-AER~~NO-DUST/CLOUD (Figure 8a), the ice crystal number density produced by ~~AER/~~DUST/CLOUD (Figure 8b) is one order higher over the simulation domain as a whole, and increased by as much as 6×10^8 /m^2 over north China and the south part of the ocean area. By contrast, the simulated cloud droplet number density produced by ~~AER/~~DUST/CLOUD (Figure 8e) is much lower than that produced by ~~NO-AER~~NO-DUST/CLOUD (Figure 8d). In ~~AER/~~DUST/CLOUD, the effects of dust reduce the cloud droplet number density by around one third over this region compared with ~~NO-AER~~NO-DUST/CLOUD (Figure 8f).

4.2.2 Vertical profile

As the spatial distributions of the ice water path and cloud water path over East Asia are altered by the effects of dust, the cloud ice mixing ratio and cloud water mixing ratio are also modified vertically. Figure 9 shows the vertical profiles of the cloud ice and cloud water mixing ratios under the combined effects of dust. Note that the vertical profiles over land, over the ocean, and over the entire simulation domain for East Asia are averaged across the whole simulation period.

Due to the effects of dust, the cloud ice mixing ratio is increased at all altitudes from the near-surface layer to higher than 15 km over the whole of East Asia, with two peaks located at 12 km and 6 km, as shown in Figure 9a. The smaller peak at 6 km is due to the enhanced cloud ice mixing ratio over land. The cloud ice mixing ratio is uniformly increased between 4 km and 13 km over land (Figure 9b), which results from the increase of ~~ice nuclei~~IN served by the abundant dust particles in the atmosphere. In contrast, the increase of the cloud ice mixing ratio over the ocean from 7 km to 15 km, with a significant peak located at 12 km (Figure 9c). The enhancement of cloud ice mixing ratio over the ocean is much greater than over land, likely due to more water vapor over the ocean. As noted above, the enhancement of the cloud ice mixing ratio over the ocean also occurs at a higher altitude (7 km to 15 km) than that over land. A possible cause of this difference is that only those particles fined enough to be lifted to high altitudes can be transported as far as the open ocean of the West Pacific, whereas over land, more dust particles with larger sizes are suspended in lower layers before settling down to the surface.

The vertical modification of the cloud water mixing ratio due to the effects of dust is fundamentally different from that of cloud ice mixing ratio. Due to the effects of dust, the cloud water mixing ratio at low layers from the near-surface to 3 km decreases over the whole of East Asia, with the average decrease peaking at around 1.5 km (Figure 9d). The overall decrease is dominated by the reduction in the cloud water mixing ratio over the ocean (Figure 9f). The cloud water mixing ratio is also decreased over land at the same layers (Figure 9e), but by smaller magnitudes compared with the decrease over the ocean. The vertical modification of the cloud water mixing ratio suggests that the effects of dust is the significantly reduce low clouds over East Asia, especially over the ocean, where there is much more abundant water vapor for cloud formation.

To summarize Section 4.2, the effects of dust result in a general increase of cloud ice and decrease of cloud water over East Asia as a whole, whereby the increase in cloud ice is mainly concentrated at the mid- to upper troposphere, while the decrease of cloud water mostly occurs in low clouds.

The increase in cloud formation at the mid- to upper troposphere is attributed to the indirect effect of dust. The abundant ~~ice nuclei~~IN in the atmosphere served by dust particles substantially increase the amount of ice crystals in mixed-phase and ice clouds at these altitudes. In contrast, the decrease of low clouds is the result of two factors. One is the warming within the atmosphere induced by the dust, leading to a much higher saturation pressure required for atmospheric water vapor to form clouds, and a much faster evaporation rate of cloud droplets, which is due to the cloud burning effect of dust. The other factor is that the super-cooled cloud droplets in the upper layers of the troposphere freeze into ice crystals at a much higher temperature and lower relative humidity when dust particles serve as ~~ice nuclei~~IN in the atmosphere, leading to an increase of atmospheric ice water path. Given an approximately constant total amount of water vapor in the atmosphere, the increased formation of ice crystals by the freezing of cloud droplets results in a reduction in the amount of liquid cloud, and thus the atmospheric cloud water path, over East Asia as a whole. The redistribution of atmospheric water vapor further strengthens the cloud radiative effect and modifies the radiation budget over East Asia, as discussed in Section 4.1.2.

4.3 Vertical temperature profile

Due to the radiative forcing directly induced by dust discussed in Section 4.1.1, and the cloud radiative effect enhanced by dust discussed in Section 4.1.2, the vertical temperature profile is modified. Figure 10 shows the modifications of the vertical temperature profiles induced by the direct radiative effect of dust, the cloud radiative effect enhanced by dust, and the full radiative effect of dust over the whole of East Asia, over land, and over the ocean during the investigated period.

On average, the temperature over the simulation domain as a whole is slightly increased in the near-surface atmosphere, decreased from 1 km to 3 km, increased significantly from 1 km up to 13 km, and then decreased above 13 km (Figure 10a). The contributions of the direct radiative effect of dust and dust-enhanced cloud radiative effect to the vertical temperature modification are shown in Figure 10b and c. The direct radiative effect of dust (Figure 10b) results in a decrease of temperature at the near-surface layer, and an increase above 1 km. In contrast, the pattern of the vertical temperature modification caused by dust-enhanced cloud radiative effect (Figure 10c) is similar to that caused by the full effect of dust, and is one order of magnitude larger magnitude than that caused by the direct radiative effect of dust.

As the radiative forcing induced by dust over land differs from that over the ocean, the effects on the vertical temperature profile requires further discussion. The decrease in temperature at the lower level of the troposphere mainly occurs over land. The temperature over land decreases significantly below 2 km, then increases gradually from 2 km to 12 km, and decreases again over 12 km (Figure 10d). The decrease in temperature at the lower level is composed of roughly equal contributions from the direct radiative effect and the dust-enhanced cloud radiative effect. However, the increase in the temperature between 2 km and 12 km is mainly attributable to the dust-enhanced cloud radiative effect (Figure 10f), the contribution of which is one order larger than that of the direct radiative effect of dust (Figure 10e). The decrease in temperature at lower layers is mainly attributable to the negative SW radiative forcing at the surface induced by dust, and the increase of temperature at the mid- to upper troposphere is due to the absorption of LW radiation by dust-enhanced ice clouds.

The modification of the vertical temperature profile over the ocean is similar to that over East Asia as a whole, especially at lower layers from the surface to 3 km, with an increase in temperature at the near-surface below 2 km, and a decrease in temperature from 1 km to 3 km (Figure 10g). The direct radiative effect of dust results in a slight decrease in temperature at the surface and at altitudes from 7 km to 9 km, but a slight increase from 1 km to 7 km and above 10 km (Figure 10h). The dust-enhanced cloud radiative effect causes an overall increase in temperature from the surface to 13 km, with a minor peak at an altitude of 1 km and a major peak at an altitude of 11 km (Figure 10i). The modification of the vertical temperature profile over the ocean is mostly contributed by the dust-enhanced cloud radiative effect over the ocean, with an almost identical pattern and magnitude to the temperature variation over East Asia as a whole (Figure 10i).

The patterns of vertical temperature modification over land and ocean are due to different mechanisms. The vertical temperature profile over land is chiefly modified by the direct radiative effect of dust at lower layers, and by the enhanced cloud radiative effect due to the greater amount of ice clouds at the mid- to upper troposphere. With a heavier dust burden over land, the SW radiation is blocked more effectively from reaching the land surface than the ocean surface. Furthermore, the temperature at the near-surface layer over land responds to the SW radiation much faster than that over the ocean, leading to a greater temperature decrease at lower levels over land. In the mid- to upper troposphere, the greater amount of ice cloud leads to greater absorption of LW radiation emitted by the Earth, and the enhanced freezing of cloud droplets into ice crystals promotes the release of latent heat, leading to a significant increase of temperature in the surrounding atmosphere. The decrease in temperature below 2 km and the increase in temperature above 2 km are likely to reduce atmospheric instability, which in turn will weakens the convective motions over land.

The mechanism for the modification of the vertical temperature profile over the ocean is more complicated. As discussed in Section 4.2, the effects of dust result in a substantial reduction of clouds, especially low clouds, and a marked increase of ice clouds at the mid- to upper troposphere over the ocean. As ice clouds are much less efficient in blocking solar radiation than low clouds, the reduction of low clouds leads to an increase of SW radiation over the ocean, which heats up the ocean surface and near-surface layer of the atmosphere. Conversely, the reduction of low clouds between 1 km and 3 km results in less LW radiation being absorbed by low clouds, and also less latent heat being released by the condensation of water vapor into cloud droplets, both of which lead to a significant decrease of temperature at layers between 1 km and 3 km. The increase in temperature above 3 km has the same cause as that over land. The greater amount of ice clouds in the mid- to upper troposphere is able to absorb more of the LW radiation emitted by the Earth, and the enhanced freezing of cloud droplets into ice crystals promotes the release of latent heat into the surrounding atmosphere, leading to a significant increase in temperature in these layers. The cooling below 1 km and warming between 1 km and 3 km are likely to enhance atmospheric instability, causing stronger convective motions over the ocean.

4.4 Atmospheric stability

As discussed above, the radiative forcing and the re-distribution of atmospheric water content induced by dust result in a modification of the vertical temperature profile over East Asia. The corresponding shift of the thermal energy in the atmosphere eventually lead to a modification of the atmospheric stability over this region.

The K-index (*KI*) is a metric widely used in meteorology to evaluate atmospheric stability, and is calculated with the following equation (George, 2014):

$$KI = T_{850} - T_{500} + Td_{850} - (T_{700} - Td_{700}) \quad (10)$$

where T_{850}, T_{700}, and T_{500} are the respective temperatures at 850 hPa, 700 hPa, and 500 hPa, and Td_{850} and Td_{700} are the dew points at 850 hPa and 700 hPa. The calculation of *KI* considers the atmospheric stability as a function of the vertical temperature lapse rate, the moisture content of the lower atmosphere, and the vertical extent of the moist layer. The larger the value of *KI*, the more unstable the atmosphere. To evaluate the effect of dust on atmospheric stability, *KI* was calculated from the simulation outputs.

Figure 11 shows the spatial distributions for the mean *KI* from ~~NO-AER~~NO-DUST/CLOUD over East Asia during the simulation period, which represents the intrinsic average atmospheric stability free from the effects of dust, and Figure 12 shows the spatial distributions for the mean difference in *KI* between ~~AER/~~DUST/NO-CLOUD and ~~NO-AER~~NO-DUST/NO-CLOUD (Figure 12a), between ~~AER/~~DUST/CLOUD and ~~NO-AER~~NO-DUST/CLOUD (Figure 12b), and between ~~AER/~~DUST/CLOUD and ~~NO-AER~~NO-DUST/ CLOUD (Figure 12c). The differences represent the modification in *KI* induced by the direct radiative effect of dust in Figure 12a, semi-direct and indirect effects, including cloud radiative effects and re-distribution of atmospheric water content enhanced by dust, in Figure 12b, and the combined effects of the previous two in Figure 12c.

As shown in Figure 11, the mean *KI* over East Asia is lower in the north and increases gradually from north to south, with the highest values located over the South China Sea and Southeast Asia, and the lowest values over the Central to North Pacific.

Under the full effects of dust, the mean modification of *KI* over most land areas in East Asia is a significant decrease. The largest decrease occurs over the dust source regions and central to East China (Figure 12c), and results from the vertical modification over land. In contrast, *KI* significantly increases over most areas of the ocean and South China, due to the different effects of dust on the vertical temperature over these areas, as discussed in Section 4.3. The contributions of the direct radiative effect of dust and the indirect effects of dust on the modification of the mean KI are shown in Figure 12a and b. The direct radiative effect of dust is to inhibit the atmospheric instability is inhibited over most land areas, indicated by a significant decrease of the mean *KI*, as shown in Figure 12a. However, the overall modification of mean *KI* is even greater over the ocean when the semi-direct and indirect effects of dust are taken into account. Upon considering the semi-direct and indirect effects of dust, the modification of *KI* is much greater over areas with more water vapor in the simulation domain, such as South China and most ocean areas, as shown in Figure 12b.

Formatted: Font: Italic

Formatted: Font: Italic

Formatted: Font: Italic

Formatted: Font: Italic

Formatted: Font: Italic

Overall, the atmosphere is significantly stabilized over the dust source regions and central to East China, but significantly destabilized over South China and most ocean areas, due to the effects of dust. The dust-enhanced cloud radiative forcing and the re-distribution of atmospheric water content due to dust contribute much more to the modification of atmospheric stability than the direct radiative effect of dust does, especially over areas with abundant water vapor.

4.5 Precipitation

The modification of atmospheric stability and re-distribution of atmospheric water content induced by dust eventually alter the precipitation over East Asia. The spatial distributions for the mean precipitation rate, including total precipitation, convective precipitation, and non-convective precipitation from ~~NO-AER~~NO-DUST/CLOUD and ~~AER/~~DUST/CLOUD, as well as the difference between the two simulations, are shown in Figure 13. Note that the precipitation rate shown in Figure 14 is the mean daily precipitation rate averaged over the simulation period.

The spatial pattern of the mean total precipitation rate from ~~NO-AER~~NO-DUST/CLOUD shown in Figure 13a is generally similar to that from ~~AER/~~DUST/CLOUD shown in Figure 13b. However, as discussed in Section 3.2.2, the simulated precipitation center produced in ~~NO-AER~~NO-DUST/NO-CLOUD spans an area from Hunan to Jiangxi (Figure 13a), to the north of the observed precipitation, and the simulated precipitation rate over South China is significantly lower than the observational values. By contrast, in ~~AER/~~DUST/CLOUD (Figure 13b), the precipitation band from Hunan to Jiangxi is markedly inhibited, while the precipitation rate over South China is enhanced, which is clearly more consistent with the observations. As shown in Figure 13c, the total precipitation is reduced by as much as 1 mm/day or more over most land areas, but increased by up to 1 mm/day over South China, due to the effects of dust. The modifications in precipitation account for over 20% of the total simulated precipitation rate over both land and the ocean.

The simulated convective precipitation mostly occurs over the southern part of the simulation domain, with precipitation centers located over central to East China, South China, the South China Sea, and Southeast Asia (Figure 13d and e). The total precipitation over these areas is chiefly affected by the modification of convective precipitation. Due to the effects of dust, convective precipitation is significantly reduced at the precipitation center from central to East China, but substantially enhanced over South China and the ocean (Figure 13f). The inhibition of convective precipitation over Central to East China has two reasons. One is the general enhancement of atmospheric stability, which reduces the convective motion over this region. The other is the decrease in low clouds over South China and the ocean, which reduces the availability of cloud droplets that can grow into rain droplets under the same meteorological conditions. The greater convective precipitation over South China is due to the greater atmospheric instability, which promotes convective motions.

The simulated non-convective precipitation is produced by the microphysics scheme. The Non-convective precipitation mainly occurs at the western rim of the Taklimakan Desert, northeast China, Japan, and the areas between 27°N and 36°N over East Asia during the simulation period. The non-convective precipitation rate produced in ~~AER/~~DUST/CLOUD (Figure 13h) is markedly lower than that produced in ~~NO-AER~~NO-DUST/CLOUD (Figure 13g) at the northern precipitation centers. Figure 13i shows that the non-convective precipitation rate is reduced by more than 30% at the western of the Taklimakan Desert and in the rain band from East China to Japan. More super-cooled water droplets can freeze into ice crystals in the upper troposphere due to the abundant ~~ice nuclei~~IN served by dust particles, leading to much lower atmospheric cloud water content and cloud droplet number concentration directly above the non-convective precipitation center. Furthermore, the warming within the atmosphere, which is caused by radiative forcing and latent heat released by the freezing of super-cooled water droplets, results in a higher saturation pressure for water vapor and faster evaporation rate for cloud droplets. This, in turn, suppresses the growth of cloud droplets into rain droplets, leading to an inhibition of non-convective precipitation. Conversely, the increase in cloud ice in some cases leads to more precipitation. The ice crystals in mixed-phase clouds can grow large enough to induce precipitation given sufficient water vapor in the atmosphere. An example is the enhancement of non-convective precipitation over the East China Sea.

5 Conclusions

By applying the updated WRF-Chem, which is capable of evaluating indirect effect of dust along with the direct and semi-direct effect in dust simulations, the full effects of dust, including direct radiative, cloud radiative, and indirect microphysical effects, on the meteorological field over East Asia during March and April 2012 were quantified and discussed.

For the radiative forcing induced by dust, the direct radiative effect of dust combined with the dust-enhanced cloud radiative effect causes a net loss of radiation at the Earth's surface, but a net gain of radiation within the atmosphere, leading to cooling at the surface and lower troposphere, and warming in the mid- to upper troposphere. The radiative forcing caused by the dust-enhanced cloud radiative effect is much greater than that caused by the direct radiative effect of dust, especially for LW radiative forcing, which is highly affected by cloud cover. The LW radiative forcing caused by the dust-enhanced cloud radiative effect is one order stronger than that cased by the direct radiative effect of dust at the top of the atmosphere and within the atmosphere. The spatial distribution of radiative forcing further implies a shift of the spatial distribution of cloud cover, such that the cloud cover is likely increased over land, but reduced over the ocean, due to the presence of dust, indicating a re-distribution of atmospheric water vapor over East Asia.

The atmospheric ice water path and ice crystal number density are significantly increased over East Asia, when abundant dust particles are available to serve as ~~ice nuclei~~IN. By contrast, the atmospheric cloud water path and cloud droplet number density are substantially reduced. Vertically, the effects of dust result in a general increase of cloud ice and decrease of cloud water over East Asia as a whole, whereby the increase of cloud ice is mainly concentrated at the mid- to upper troposphere, while the decrease in cloud water mostly occurs in low clouds. The increase in clouds at the mid- to upper troposphere is due to the indirect effect of dust by serving as ~~ice nuclei~~IN. The reduction in low clouds is attributed to two factors. One is the semi-direct effect of dust. Dust particles within clouds absorb radiation and warm up the surrounding environment, leading to a much greater saturation pressure required for atmospheric water vapor to form clouds, and a much faster evaporation rate of cloud droplets. The other factor is that the ice nucleation process enhanced by dust facilitates the freezing of atmospheric super-cooled water droplets into ice crystals.

The radiative forcing and re-distribution of atmospheric water vapor induced by dust lead to a modification of the vertical temperature profile. Consequently, the atmosphere is stabilized over most land areas, but destabilized over most of the ocean in East Asia. The cloud radiative forcing enhanced by dust and the re-distribution of atmospheric water content due to dust contribute much more to the modification of atmospheric stability than the direct radiative effect of dust does.

Convective precipitation is inhibited over most land areas in East Asia, because of the enhanced atmospheric stability, and the reduction in cloud droplets capable of growing into rain droplets under atmospheric conditions. Conversely, convective precipitation is enhanced over South China and the ocean due to the greater atmospheric instability over these areas. The presence of much fewer cloud droplets in the atmosphere, combined with the atmospheric warming caused by radiative forcing and the release of latent heat by the freezing of super-cooled water droplets, results in a higher saturation pressure for water vapor and faster evaporation rate for cloud droplets, which in turn inhibit non-convective precipitation. The decrease in convective and non-convective precipitation results in a reduction of total precipitation over East Asia. Nevertheless, the increase of cloud ice also leads to more precipitation in some cases. The ice crystals in mixed-phase clouds can grow large enough to induce a precipitation given sufficient atmospheric water vapor.

Acknowledgement. We would like to acknowledge the principle investigators and their staff from Data Assimilation and Modeling Center for Tibetan Multi-spheres, Institute of Tibetan Plateau Research, Chinese Academy of Sciences, for provision of the China Meteorological Forcing Dataset used in this study for model validation. The dataset can be found online at http://westdc.westgis.ac.cn/data/7a35329c-c53f-4267-aa07-e0037d913a21. Lin Su would like to thank Dr. Georg Grell, Dr. Stuart McKeen, and Dr. Ravan Ahmandov from the Earth System Research Laboratory, U.S. National Oceanic and Atmospheric Administration for insightful discussions. All data used in this paper are properly cited and referred to in the reference list. All data shown in the results are available upon request. This work was supported by NSFC/RGC Grant N_HKUST631/05, NSFC-FD Grant U1033001, and the RGC Grant 16303416.

References

Atkinson, J. D., Murray, B. J., Woodhouse, M. T., Whale, T. F., Baustian, K. J., Carslaw, K. S., Dobbie, S., O'sullivan, D., and Malkin, T. L.: The importance of feldspar for ice nucleation by mineral dust inmixed-phase clouds, Nature, 498, 355, 2013.

Bi, J., Huang, J., Fu, Q., Ge, J., Shi, J., Zhou, T., and Zhang, W.: Field measurement of clear-sky solar irradiance in Badain Jaran Desert of Northwestern China, Journal of Quantitative Spectroscopy and Radiative Transfer, 122, 194-207, 2013.

Bigg, E.: The formation of atmospheric ice crystals by the freezing of droplets, Quarterly Journal of the Royal Meteorological Society, 79, 510-519, 1953.

Broadley, S., Murray, B., Herbert, R., Atkinson, J., Dobbie, S., Malkin, T., Condliffe, E., and Neve, L.: Immersion mode heterogeneous ice nucleation by an illite rich powder representative of atmospheric mineral dust, Atmospheric Chemistry and Physics, 12, 287-307, 2012.

Chen, Y., Yang, K., He, J., Qin, J., Shi, J., Du, J., and He, Q.: Improving land surface temperature modeling for dry land of China, Journal of Geophysical Research: Atmospheres, 116, 2011.

Connolly, P., Möhler, O., Field, P., Saathoff, H., Burgess, R., Choularton, T., and Gallagher, M.: Studies of heterogeneous freezing by three different desert dust samples, Atmospheric Chemistry and Physics, 9, 2805-2824, 2009.

DeMott, P. J., Sassen, K., Poellot, M. R., Baumgardner, D., Rogers, D. C., Brooks, S. D., Prenni, A. J., and Kreidenweis, S. M.: African dust aerosols as atmospheric ice nuclei, Geophysical Research Letters, 30, 2003.

DeMott, P. J., Prenni, A. J., McMeeking, G. R., Sullivan, R. C., Petters, M. D., Tobo, Y., Niemand, M., Möhler, O., Snider, J. R., and Wang, Z.: Integrating laboratory and field data to quantify the immersion freezing ice nucleation activity of mineral dust particles, Atmospheric Chemistry and Physics, 15, 393-409, 2015.

Ge, J., Su, J., Ackerman, T., Fu, Q., Huang, J., and Shi, J.: Dust aerosol optical properties retrieval and radiative forcing over northwestern China during the 2008 China - US joint field experiment, Journal of Geophysical Research: Atmospheres, 115, 2010.

George, J. J.: Weather forecasting for aeronautics, Academic press, 2014.

Ginoux, P., Chin, M., Tegen, I., Prospero, J. M., Holben, B., Dubovik, O., and Lin, S. J.: Sources and distributions of dust aerosols simulated with the GOCART model, Journal of Geophysical Research: Atmospheres, 106, 20255-20273, 2001.

Ginoux, P., Prospero, J. M., Torres, O., and Chin, M.: Long-term simulation of global dust distribution with the GOCART model: correlation with North Atlantic Oscillation, Environmental Modelling & Software, 19, 113-128, 2004.

Grell, Ahmadov, R., Peckham, S., Wong, K., Zhang, L., McKeen, S. A., Easter, R., Fast, J. D., Gustafson, W., Ma, P. L., Singh, B., Hodzic, A., Batrth, M., Pfster, G., Wolters, S., Bella, M., Freitas, S. R., Tuccella, P., Zhang, Y., Wang, K., and Klose, M.: WRF-Chem V3. 8: A summary of status and updates, EGU General Assembly Conference Abstracts, 2016.

Grell, G. A., and Freitas, S. R.: A scale and aerosol aware stochastic convective parameterization for weather and air

Formatted: Line spacing: 1.5 lines

Formatted: Font: (Default) Times New Roman

Formatted: Font: (Default) Cambria Math

Formatted: Font: (Default) Times New Roman

quality modeling, Atmos. Chem. Phys, 14, 5233-5250, 2014.

Hansen, J., Sato, M., and Ruedy, R.: Radiative forcing and climate response, Journal of Geophysical Research: Atmospheres, 102, 6831-6864, 1997.

Hartmann, D., Tank, A., and Rusticucci, M.: IPCC fifth assessment report, climate change 2013: The physical science basis, IPCC AR5, 31-39, 2013.

Hoose, C., Lohmann, U., Erdin, R., and Tegen, I.: The global influence of dust mineralogical composition on heterogeneous ice nucleation in mixed-phase clouds, Environmental Research Letters, 3, 025003, 2008.

Huang, J., Fu, Q., Su, J., Tang, Q., Minnis, P., Hu, Y., Yi, Y., and Zhao, Q.: Taklimakan dust aerosol radiative heating derived from CALIPSO observations using the Fu-Liou radiation model with CERES constraints, Atmospheric Chemistry and Physics, 9, 4011-4021, 2009.

Huang, J.: Emission, transport, and radiative effects of mineral dust from the Taklimakan and Gobi deserts: comparison of measurements and model results, Atmos. Chem. Phys, 1680, 7324, 2017.

Iacono, M. J., Delamere, J. S., Mlawer, E. J., Shephard, M. W., Clough, S. A., and Collins, W. D.: Radiative forcing by long‐lived greenhouse gases: Calculations with the AER radiative transfer models, Journal of Geophysical Research: Atmospheres, 113, 2008.

Janjić, Z. I.: The step-mountain eta coordinate model: Further developments of the convection, viscous sublayer, and turbulence closure schemes, Monthly Weather Review, 122, 927-945, 1994.

Janjić, Z. I.: Nonsingular implementation of the Mellor–Yamada level 2.5 scheme in the NCEP Meso model, NCEP office note, 437, 61, 2002.

Karydis, V., Kumar, P., Barahona, D., Sokolik, I., and Nenes, A.: On the effect of dust particles on global cloud condensation nuclei and cloud droplet number, Journal of Geophysical Research: Atmospheres, 116, 2011.

Koehler, K., Kreidenweis, S., DeMott, P., Petters, M., Prenni, A., and Möhler, O.: Laboratory investigations of the impact of mineral dust aerosol on cold cloud formation, Atmospheric Chemistry and Physics, 10, 11955-11968, 2010.

Koop, T., Luo, B., Tsias, A., and Peter, T.: Water activity as the determinant for homogeneous ice nucleation in aqueous solutions, Nature, 406, 611-614, 2000.

Lacis, A.: Climate forcing, climate sensitivity, and climate response: A radiative modeling perspective on atmospheric aerosols, Aerosol forcing of climate, 11-42, 1995.

Liu, Huang, J., Shi, G., Takamura, T., Khatri, P., Bi, J., Shi, J., Wang, T., Wang, X., and Zhang, B.: Aerosol optical properties and radiative effect determined from sky-radiometer over Loess Plateau of Northwest China, Atmospheric Chemistry and Physics, 11, 11455-11463, 2011a.

Liu, Zheng, Y., Li, Z., Flynn, C., Welton, E. J., and Cribb, M.: Transport, vertical structure and radiative properties of dust events in southeast China determined from ground and space sensors, Atmospheric environment, 45, 6469-6480, 2011b.

Lohmann, U., and Feichter, J.: Global indirect aerosol effects: a review, Atmospheric Chemistry and Physics, 5, 715-737, 2005.

Lohmann, U., and Diehl, K.: Sensitivity studies of the importance of dust ice nuclei for the indirect aerosol effect on stratiform mixed-phase clouds, Journal of the Atmospheric Sciences, 63, 968-982, 2006.

Formatted: Font: (Default) Cambria Math

Formatted: Font: (Default) Times New Roman

Mallet, M., Tulet, P., Serça, D., Solmon, F., Dubovik, O., Pelon, J., Pont, V., and Thouron, O.: Impact of dust aerosols on the radiative budget, surface heat fluxes, heating rate profiles and convective activity over West Africa during March 2006, Atmospheric Chemistry and Physics, 9, 7143-7160, 2009.

Mlawer, E. J., Taubman, S. J., Brown, P. D., Iacono, M. J., and Clough, S. A.: Radiative transfer for inhomogeneous atmospheres: RRTM, a validated correlated‐k model for the longwave, Journal of Geophysical Research: Atmospheres, 102, 16663-16682, 1997.

Nabat, P., Somot, S., Mallet, M., Michou, M., Sevault, F., Driouech, F., Meloni, D., Di Sarra, A., Di Biagio, C., and Formenti, P.: Dust aerosol radiative effects during summer 2012 simulated with a coupled regional aerosol–atmosphere–ocean model over the Mediterranean, Atmospheric Chemistry and Physics, 15, 3303-3326, 2015a.

Nabat, P., Somot, S., Mallet, M., Sevault, F., Chiacchio, M., and Wild, M.: Direct and semi-direct aerosol radiative effect on the Mediterranean climate variability using a coupled regional climate system model, Climate dynamics, 44, 1127-1155, 2015b.

Palacios, L., Baró, R., and Jiménez-Guerrero, P.: An on-line modelling study of the direct effect of atmospheric aerosols over Europe, Física de la Tierra, 27, 155, 2015.

Perlwitz, J., and Miller, R. L.: Cloud cover increase with increasing aerosol absorptivity: A counterexample to the conventional semidirect aerosol effect, Journal of Geophysical Research: Atmospheres, 115, 2010.

Phillips, V. T., DeMott, P. J., and Andronache, C.: An empirical parameterization of heterogeneous ice nucleation for multiple chemical species of aerosol, Journal of the atmospheric sciences, 65, 2757-2783, 2008.

Pinker, R., and Laszlo, I.: Modeling surface solar irradiance for satellite applications on a global scale, Journal of Applied Meteorology, 31, 194-211, 1992.

Rodell, M., Houser, P., Jambor, U., Gottschalck, J., Mitchell, K., Meng, C., Arsenault, K., Cosgrove, B., Radakovich, J., and Bosilovich, M.: The global land data assimilation system, Bulletin of the American Meteorological Society, 85, 381-394, 2004.

Sassen, K.: Indirect climate forcing over the western US from Asian dust storms, Geophysical Research Letters, 29, 2002.

Sassen, K., DeMott, P. J., Prospero, J. M., and Poellot, M. R.: Saharan dust storms and indirect aerosol effects on clouds: CRYSTAL‐FACE results, Geophysical Research Letters, 30, 2003.

Satheesh, S., Deepshikha, S., and Srinivasan, J.: Impact of dust aerosols on Earth–atmosphere clear‐sky albedo and its short wave radiative forcing over African and Arabian regions, International Journal of Remote Sensing, 27, 1691-1706, 2006.

Seigel, R., Van Den Heever, S., and Saleeby, S.: Mineral dust indirect effects and cloud radiative feedbacks of a simulated idealized nocturnal squall line, Atmospheric Chemistry and Physics, 13, 4467-4485, 2013.

Seinfeld, J. H., Carmichael, G. R., Arimoto, R., Conant, W. C., Brechtel, F. J., Bates, T. S., Cahill, T. A., Clarke, A. D., Doherty, S. J., and Flatau, P. J.: ACE-ASIA: Regional climatic and atmospheric chemical effects of Asian dust and pollution, Bulletin of the American Meteorological Society, 85, 367-380, 2004.

Shao: Simplification of a dust emission scheme and comparison with data, Journal of Geophysical Research: Atmospheres, 109, 2004.

Formatted: Font: (Default) Cambria Math

Formatted: Font: (Default) Times New Roman

Formatted: Font: (Default) Cambria Math

Formatted: Font: (Default) Times New Roman

Formatted: Font: (Default) Cambria Math

Formatted: Font: (Default) Times New Roman

Shao, Ishizuka, M., Mikami, M., and Leys, J.: Parameterization of size-resolved dust emission and validation with measurements, Journal of Geophysical Research: Atmospheres, 116, 2011.

Sheffield, J., Goteti, G., and Wood, E. F.: Development of a 50-year high-resolution global dataset of meteorological forcings for land surface modeling, Journal of Climate, 19, 3088-3111, 2006.

Solomon, S.: Climate change 2007-the physical science basis: Working group I contribution to the fourth assessment report of the IPCC, Cambridge University Press, 2007.

Su, L., and Fung, J. C.: Sensitivities of WRF-Chem to dust emission schemes and land surface properties in simulating dust cycles during springtime over East Asia, Journal of Geophysical Research: Atmospheres, 120, 2015.

Su, L. and Fung, J. C. H.: Investigating the role of dust in ice nucleation within clouds and further effects on regional weather system over East Asia – Part I: model development and validation, Atmos. Chem. Phys. Discuss., https://doi.org/10.5194/acp-2017-754, in review, 2017.

Targino, A. C., Krejci, R., Noone, K. J., and Glantz, P.: Single particle analysis of ice crystal residuals observed in orographic wave clouds over Scandinavia during INTACC experiment, Atmospheric Chemistry and Physics, 6, 1977-1990, 2006.

Teller, A., and Levin, Z.: The effects of aerosols on precipitation and dimensions of subtropical clouds: a sensitivity study using a numerical cloud model, Atmospheric Chemistry and Physics, 6, 67-80, 2006.

Tesfaye, M., Tsidu, G. M., Botai, J., and Sivakumar, V.: Mineral dust aerosol distributions, its direct and semi-direct effects over South Africa based on regional climate model simulation, Journal of Arid Environments, 114, 22-40, 2015.

Thompson, G., and Eidhammer, T.: A study of aerosol impacts on clouds and precipitation development in a large winter cyclone, Journal of the Atmospheric Sciences, 71, 3636-3658, 2014.

Wesely, M.: Parameterization of surface resistances to gaseous dry deposition in regional-scale numerical models, Atmospheric Environment (1967), 23, 1293-1304, 1989.

Yang, K., He, J., Tang, W., Qin, J., and Cheng, C. C.: On downward shortwave and longwave radiations over high altitude regions: Observation and modeling in the Tibetan Plateau, Agricultural and Forest Meteorology, 150, 38-46, 2010.

Zhang, C., Wang, M., Morrison, H., Somerville, R. C., Zhang, K., Liu, X., and Li, J. L. F.: Investigating ice nucleation in cirrus clouds with an aerosol-enabled Multiscale Modeling Framework, Journal of Advances in Modeling Earth Systems, 6, 998-1015, 2014.

Formatted: Font: (Default) Cambria Math

Formatted: Font: (Default) Times New Roman

Formatted: Font: (Default) Cambria Math

Formatted: Font: (Default) Times New Roman

Formatted: Font: (Default) Cambria Math

Formatted: Font: (Default) Times New Roman

Formatted: Justified, Space After: 0 pt, Line spacing: 1.5 lines, No widow/orphan control

List of tables and figures

Formatted: Line spacing: 1.5 lines

Figure 10: Modification of vertical temperature profile induced by the full effects of dust (left panel), the direct radiative effect of dust (middle panel), and the semi-direct and indirect effects of dust (right panel) over the entire simulation domain (a-c), over land (d-f), and over ocean (g-i).

Figure 11: Spatial distributions of the monthly average K-index from ~~NO-AER~~NO-DUST/CLOUD.

Figure 12: Spatial distributions of the modification of K-index induced by the direct radiative effect of dust (a), the semi-direct and indirect effects of dust (b), and the full effects of dust (c).

Figure 13: Spatial distributions of the average simulated total precipitation rate (a-c), convective precipitation rate (d-f), and non-convective precipitation rate (g-i) from ~~NO-AER~~NO-DUST/CLOUD (left panel), ~~AER/~~DUST/CLOUD (middle panel), and the difference between ~~AER/~~DUST/CLOUD and ~~NO-AER~~NO-DUST/CLOUD (right panel).

Table 1: Model configurations for the numerical simulations.

Scheme \ Experiment	~~NO-AER~~NO-DUST/NO-CLOUD	~~NO-AER~~NO-DUST/CLOUD	~~AER/~~DUST/NO-CLOUD	~~AER/~~DUST/CLOUD
Dust emission scheme	----	----	Shao	Shao
~~**Soil dataset**~~	~~USGS~~	~~USGS~~	~~USGS~~	~~USGS~~
~~**Land surface model**~~	~~Noah LSM~~	~~Noah LSM~~	~~Noah LSM~~	~~Noah LSM~~
~~**Planetary boundary layer**~~	~~MYJ~~	~~MYJ~~	~~MYJ~~	~~MYJ~~
~~**Moisture convection**~~	~~Grell–Freitas~~	~~Grell–Freitas~~	~~Grell–Freitas~~	~~Grell–Freitas~~
~~**Long-wave radiation**~~	~~RRTMG~~	~~RRTMG~~	~~RRTMG~~	~~RRTMG~~
~~**Short-wave radiation**~~	~~RRTMG~~	~~RRTMG~~	~~RRTMG~~	~~RRTMG~~
~~**Microphysics**~~	~~GOCART-Thompson~~	~~GOCART-Thompson~~	~~GOCART-Thompson~~	~~GOCART-Thompson~~
~~**Chemistry mechanism**~~	~~GOCART~~	~~GOCART~~	~~GOCART~~	~~GOCART~~
Dry deposition	----	----	Gravitational settling/surface deposition	Gravitational settling/surface deposition
Wet deposition	----	----	In-cloud and below-cloud	In-cloud and below-cloud
Aerosol optical scheme	----	----	Maxwell-Garnett	Maxwell-Garnett
Aerosol radiative feedback	off	off	on	on
Cloud radiative feedback	off	on	off	on

Table 2: WRF-Chem-simulated SW, LW, and net radiative forcing (W/m^2) induced by dust over East Asia at TOA, BOT, and ATM.

	Clear-sky			**All-sky**		
	SW	LW	Net	SW	LW	Net
TOA (+down)	-1.22	0.02	-1.20	-7.81	9.52	1.70
ATM (+warm)	1.23	-1.07	0.15	0.06	9.26	9.33
BOT (+down)	-2.44	1.09	-1.36	-7.87	0.25	-7.62

SW: short-wave radiative forcing; LW: long-wave radiative forcing; Net: net radiative forcing.
TOA: radiative forcing at the top of the atmosphere; ATM: radiative effect within the atmosphere; BOT: radiative effect at the bottom of the atmosphere.

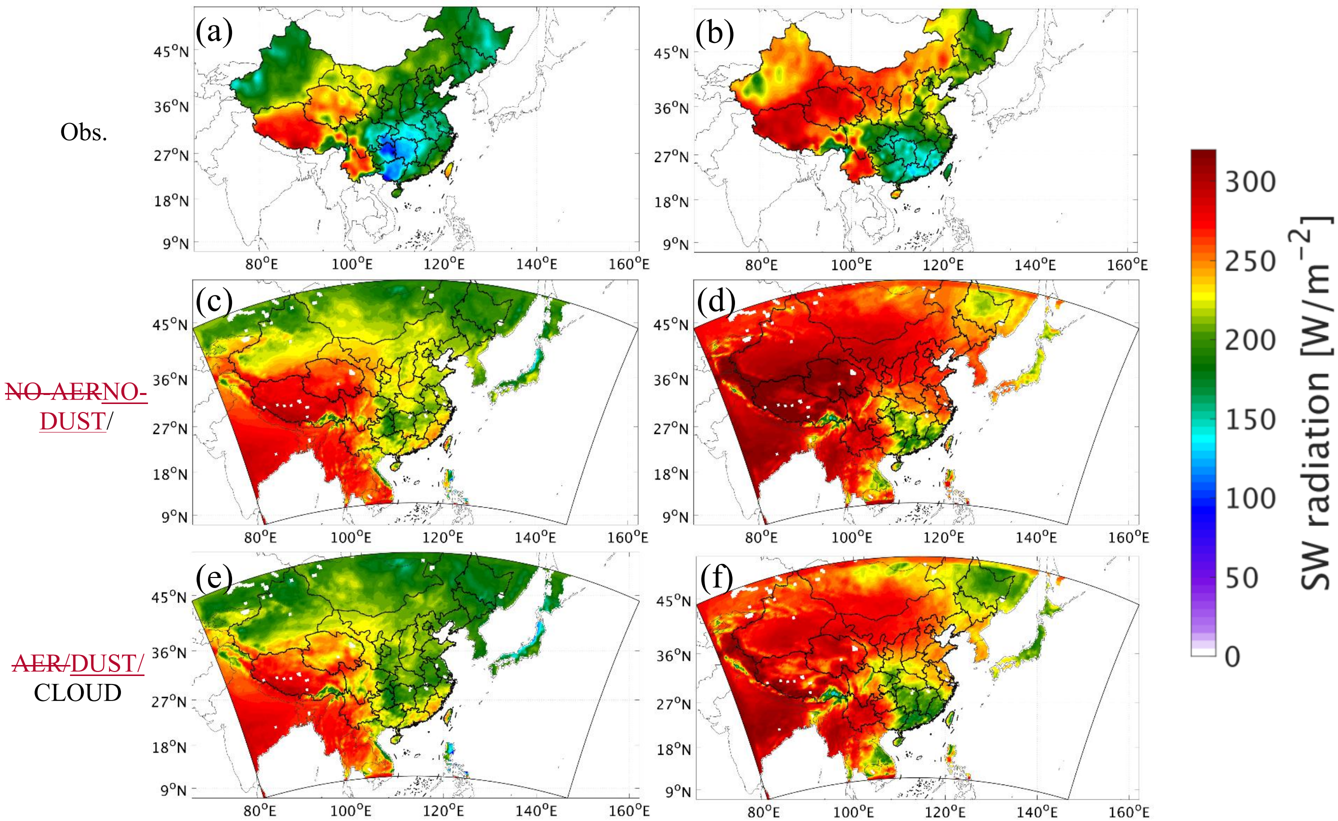

Figure 1: Spatial distributions of the average downward SW radiation at surface from observations (a, b), from ~~NO-AER~~NO-DUST/CLOUD (c, d), and from ~~AER-~~DUST-CLOUD (e, f) during March (left panel) and April (right panel) 2012.

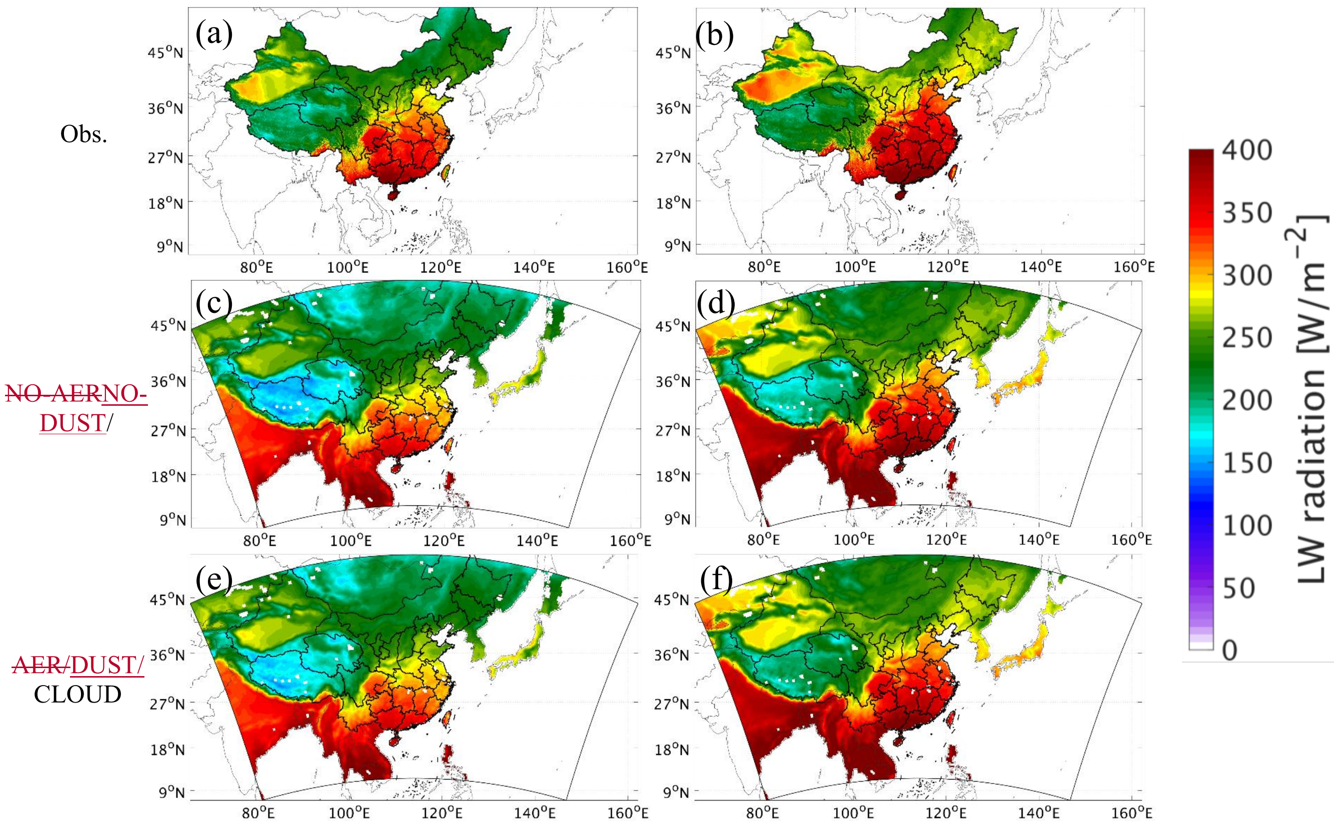

Figure 2: Spatial distributions of the average downward LW radiation at surface from observations (a, b), from ~~NO-AER~~NO-DUST/CLOUD (c, d), and from ~~AER-~~DUST-CLOUD (e, f) during March (left panel) and April (right panel) 2012.

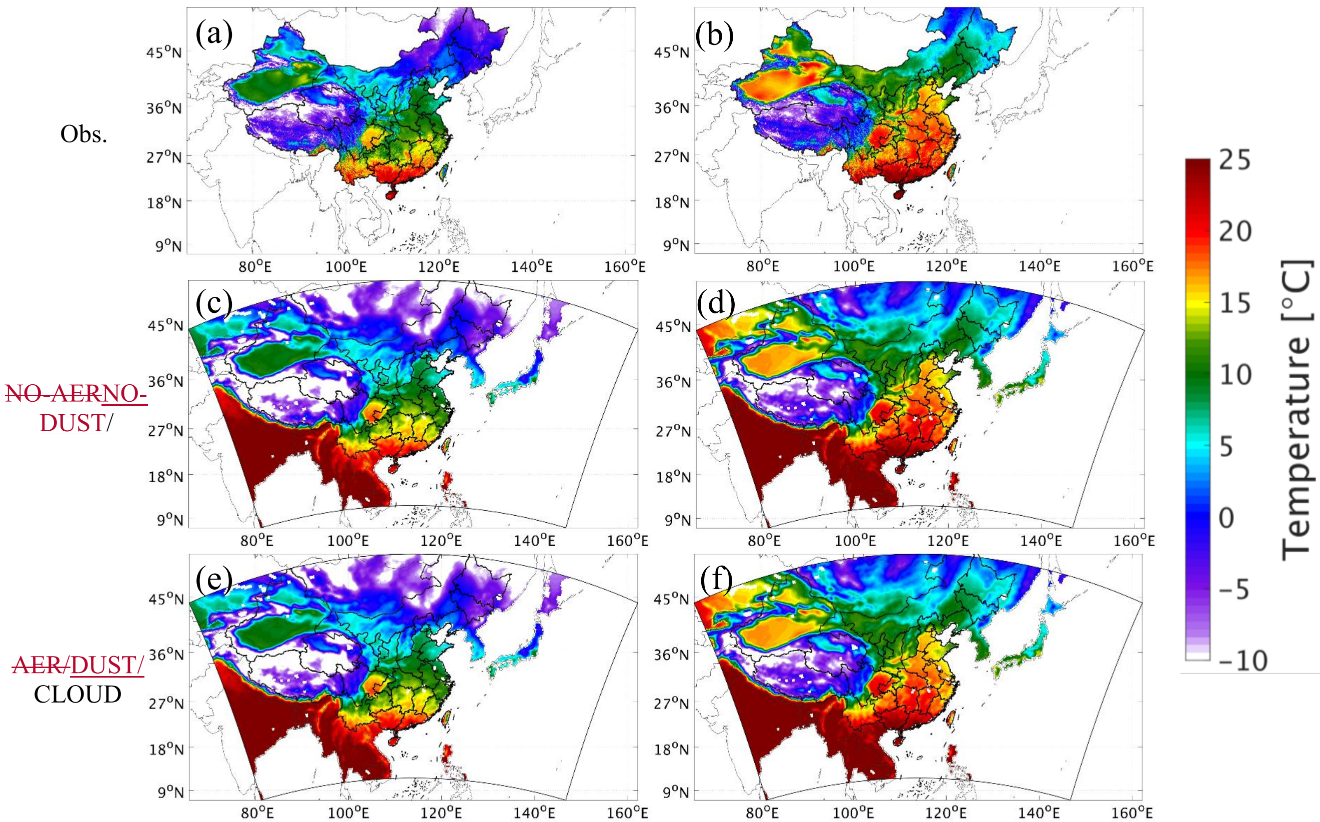

Figure 3: Spatial distributions of the average near-surface temperature from observations (a, b), from ~~NO-AER~~NO-DUST/CLOUD (c, d), and from ~~AER-~~DUST-CLOUD (e, f) during March (left panel) and April (right panel) 2012.

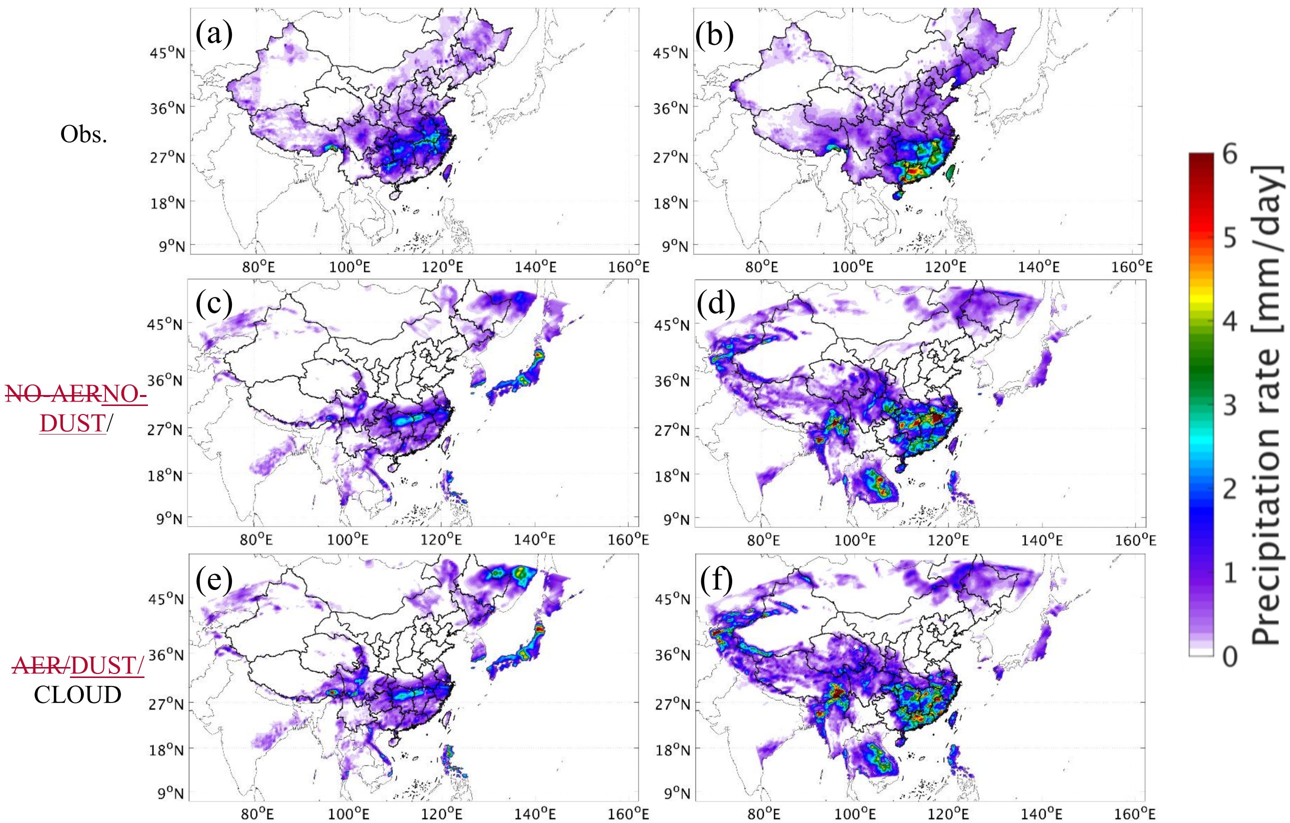

Figure 4: Spatial distributions of the average precipitation rate from observations (a, b), from ~~NO-AER~~NO-DUST/CLOUD (c, d), and from ~~AER/~~DUST/CLOUD (e, f) during March (left panel) and April (right panel) 2012.

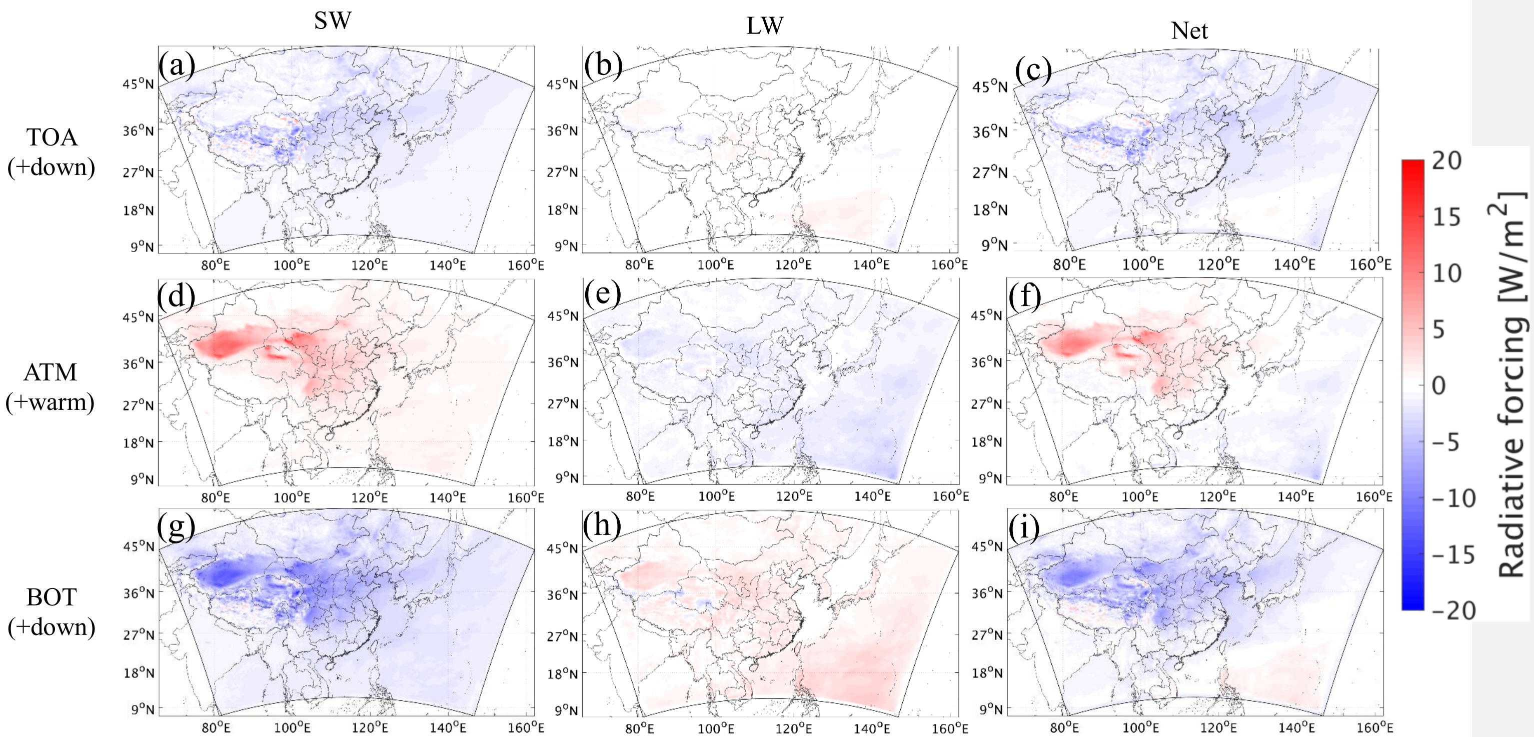

Figure 5: Spatial distributions of the clear-sky SW (left panel), LW (middle panel), and net (right panel) radiative forcing at the top of the atmosphere (TOA, a-c), within the atmosphere (ATM, d-f), and at the bottom of the atmosphere (BOT, g-i).

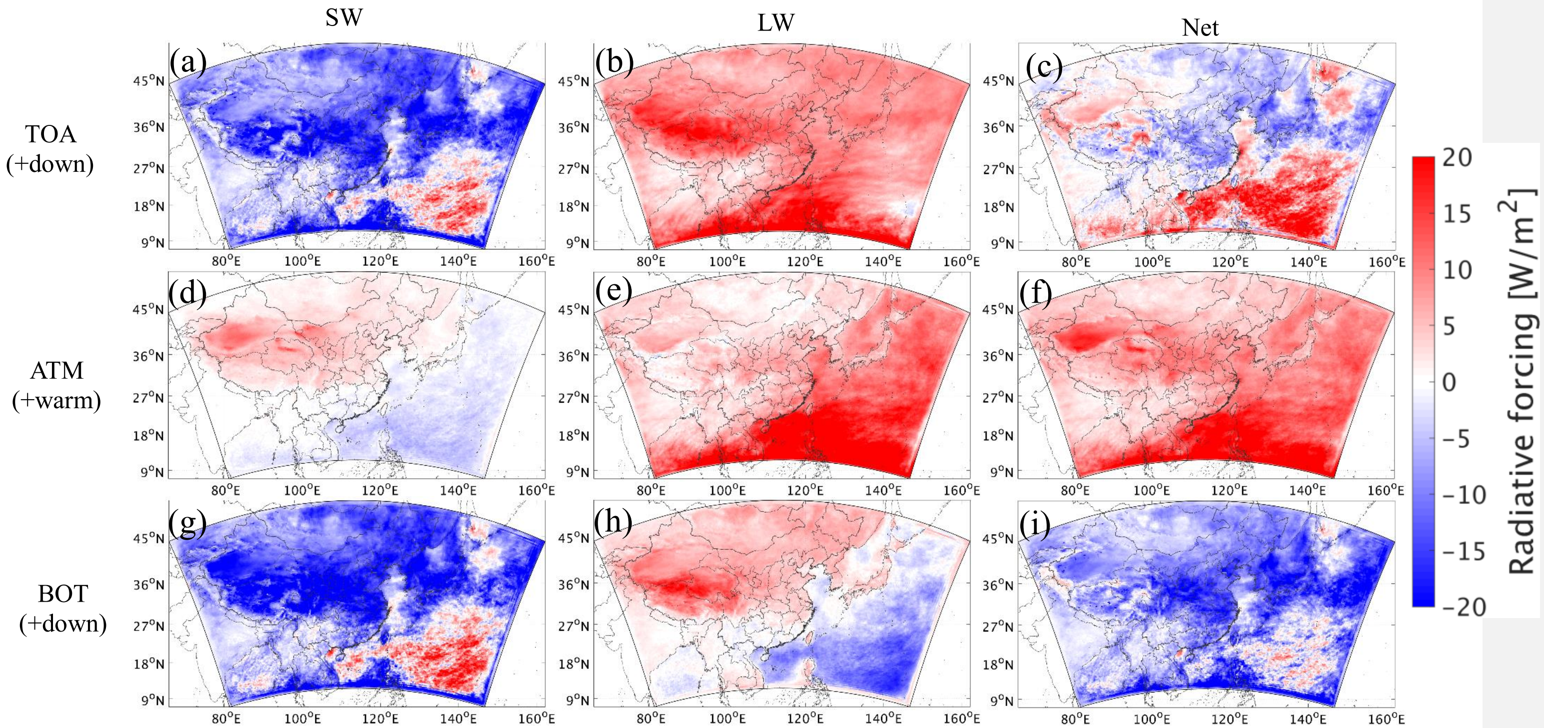

Figure 6: Spatial distributions of the all-sky SW (left panel), LW (middle panel), and net (right panel) radiative forcing at the top of the atmosphere (TOA, a-c), within the atmosphere (ATM, d-f), and at the bottom of the atmosphere (BOT, g-i).

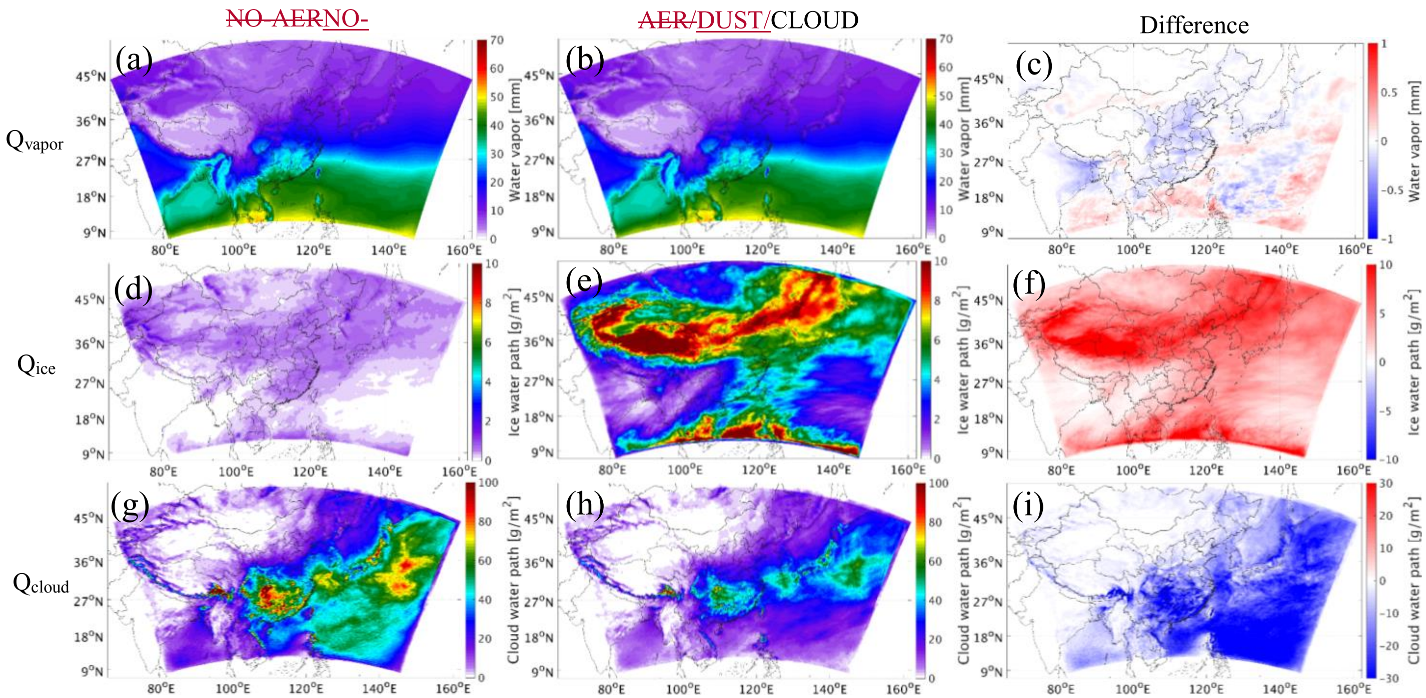

Figure 7: Spatial distributions of the average simulated precipitable water vapor (a-c), ice water path (d-f), and cloud water path (g-i) from ~~NO-AER~~NO-DUST/CLOUD (left panel), ~~AER/~~DUST/CLOUD (middle panel), and difference between ~~AER/~~DUST/CLOUD and ~~NO-AER~~NO-DUST/CLOUD (right panel).

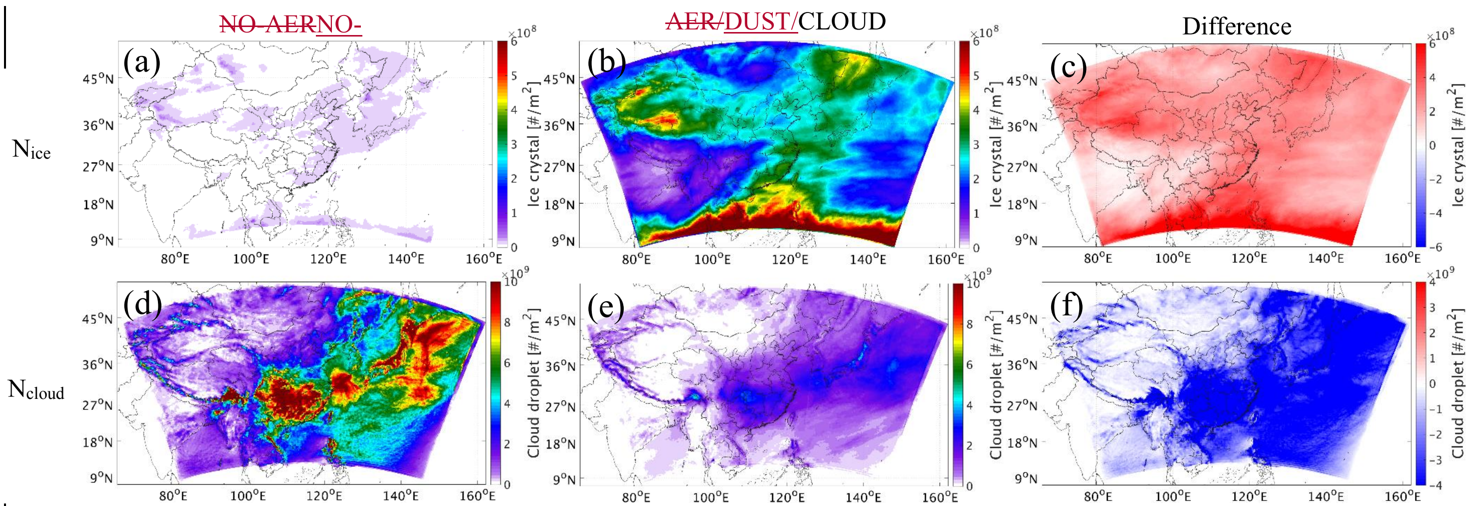

Figure 8: Spatial distributions of the average simulated ice crystal number density (a-c) and cloud droplet number density (d-f) from ~~NO-AER~~NO-DUST/CLOUD (left panel), ~~AER/~~DUST/CLOUD (middle panel), and difference between ~~AER/~~DUST/CLOUD and ~~NO-AER~~NO-DUST/NO-CLOUD (right panel).

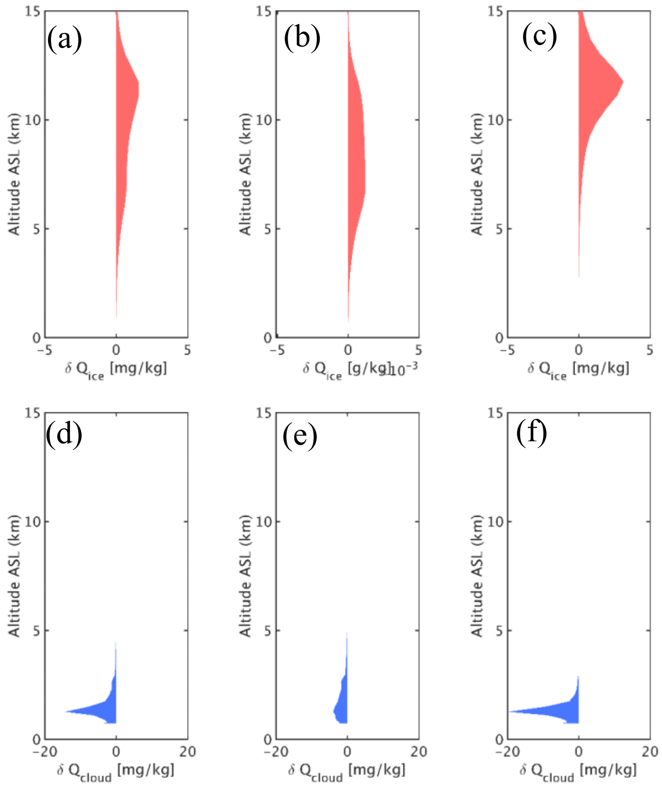

Figure 9: Vertical profile of the modification of cloud ice (a-c) and cloud water content (e-f) induced by dust over the entire simulation domain (left panel), over land (middle panel), and over ocean (right panel).

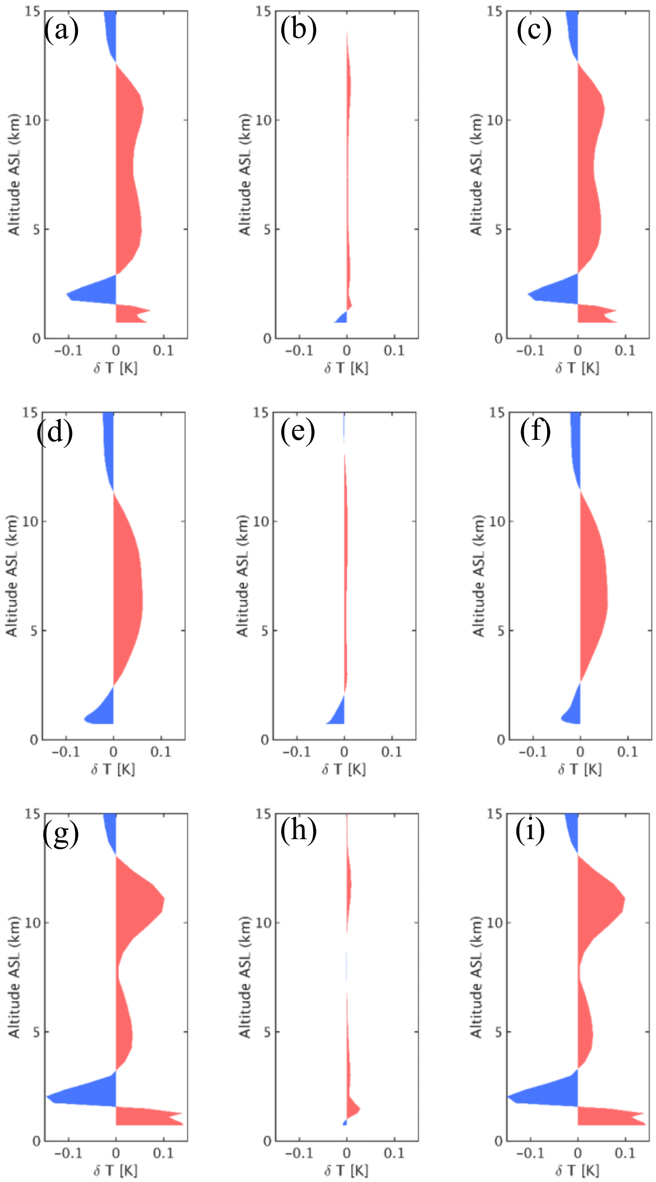

Figure 10: Modification of vertical temperature profile induced by the full effects of dust (left panel), the direct radiative effect of dust (middle panel), and the semi-direct and indirect effects of dust (right panel) over the entire simulation domain (a-c), over land (d-f), and over ocean (g-i).

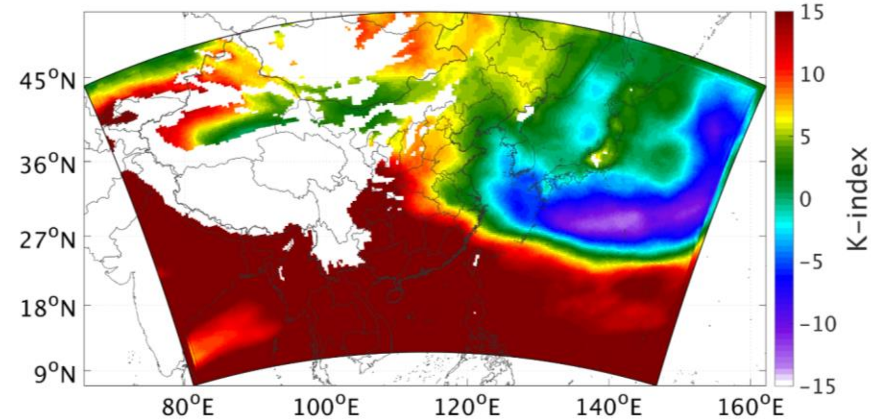

Figure 11: Spatial distributions of the monthly average K-index from ~~NO-AER~~NO-DUST/CLOUD.

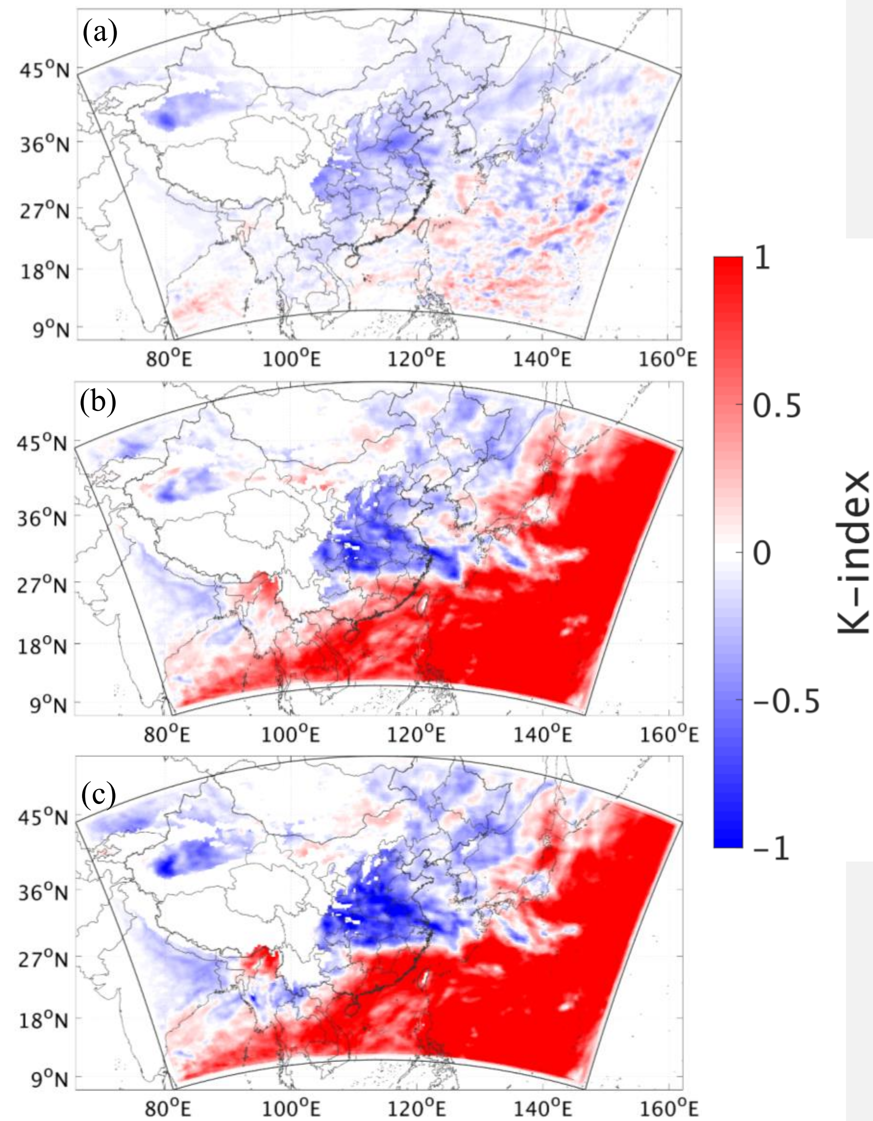

Figure 12: Spatial distributions of the modification of K-index induced by the direct radiative effect of dust (a), the semi-direct and indirect effects of dust (b), and the full effects of dust (c).

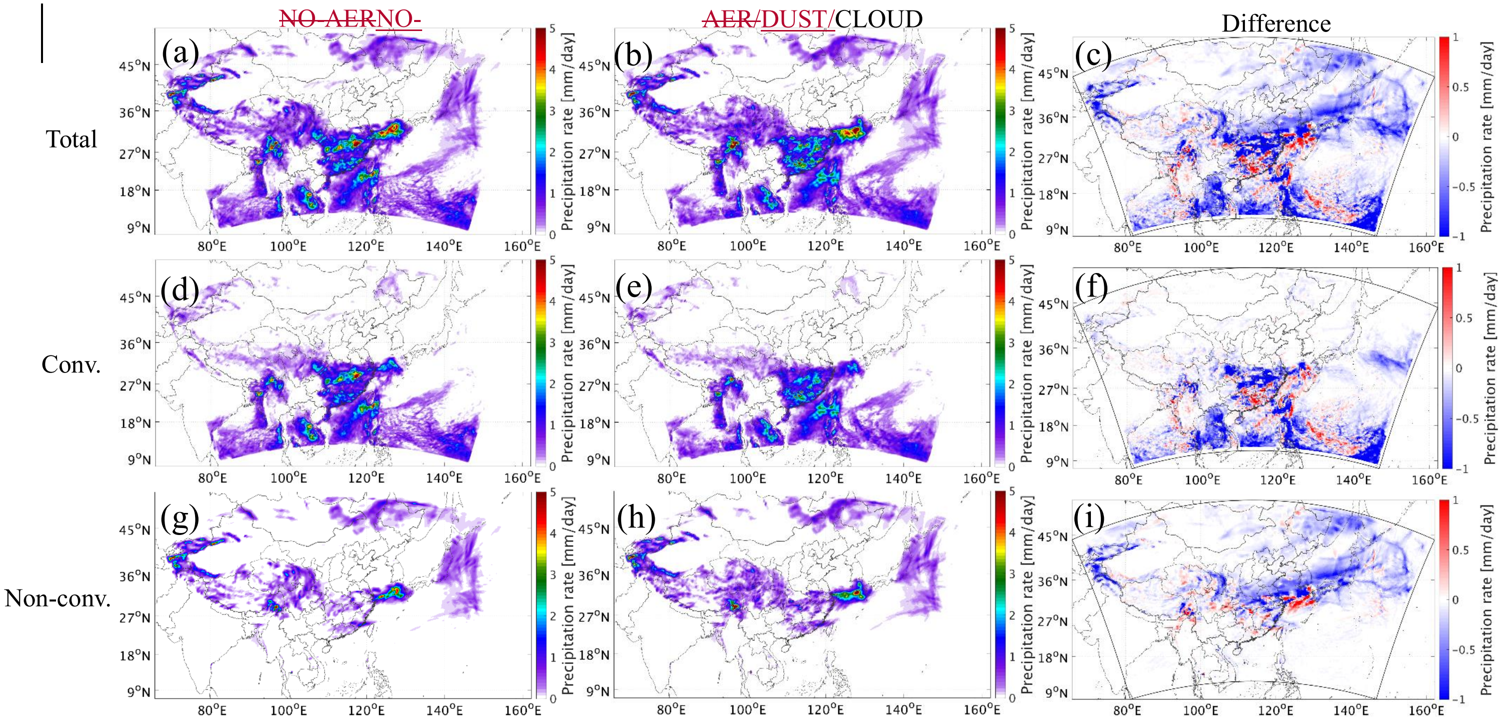

Figure 13: Spatial distributions of the average simulated total precipitation rate (a-c), convective precipitation rate (d-f), and non-convective precipitation rate (g-i) from ~~NO-AER~~NO-DUST/CLOUD (left panel), ~~AER/~~DUST/CLOUD (middle panel), and the difference between ~~AER/~~DUST/CLOUD and ~~NO-AER~~NO-DUST/CLOUD (right panel).